

The Nd Break-Up Process in Leading Order in a Three-Dimensional Approach

I. Fachruddin^{†*}, Ch. Elster[‡], W. Glöckle[†]

[†]*Institut für Theoretische Physik II, Ruhr-Universität Bochum, D-44780 Bochum, Germany.*

[‡]*Department of Physics and Astronomy, Ohio University, Athens, OH 34701, and Institut für Kernphysik, Forschungszentrum Jülich, D-52425 Jülich.*

(November 5, 2018)

Abstract

A three-dimensional approach based on momentum vectors as variables for solving the three nucleon Faddeev equation in first order is presented. The nucleon-deuteron break-up amplitude is evaluated in leading order in the NN T-matrix, which is also generated directly in three dimensions avoiding a summation of partial wave contributions. A comparison of semi-exclusive observables in the $d(p, n)pp$ reaction calculated in this scheme with those generated by a traditional partial wave expansion shows perfect agreement at lower energies. At about 200 MeV nucleon laboratory energies deviations in the peak of the cross section appear, which may indicate that special care is required in a partial wave approach for energies at and higher than 200 MeV. The role of higher order rescattering processes beyond the leading order in the NN T-matrix is investigated with the result, that at 200 MeV rescattering still provides important contributions to the cross section and certain spin observables. The influence of a relativistic treatment of the kinematics is investigated. It is found that relativistic effects become important at projectile energies higher than 200 MeV.

PACS number(s): 21.45.+v, 13.75.Cs, 25.40.Kv

Typeset using REVTEX

*Permanent address: Jurusan Fisika, Universitas Indonesia, Depok 16424, Indonesia

I. INTRODUCTION

During the last two decades calculations of nucleon-deuteron (Nd) scattering based on momentum space Faddeev equations [1] experienced enormous improvement and refinement. It is fair to state that below about 200 MeV projectile energy the momentum space Faddeev equations for three-nucleon (3N) scattering now can be solved with very high accuracy for the most modern two and three nucleon forces. A summary of these achievements is given in Ref. [2]. The approach to 3N scattering described in Ref. [2] is based on using angular momentum eigenstates for the two- and three-body system. For low projectile energies this procedure is certainly physically justified due to arguments related to the centrifugal barrier. However, to probe the strong interaction at shorter distances one has to go to higher projectile energies, where the algebraic and algorithmic work carried out in traditional partial wave (PW) decomposition can be quite involved. A more crucial hurdle is posed by the fact that in three-nucleon scattering (3N) calculations for projectile energies of a few hundred MeV the number of partial waves needed to achieve numerical convergence proliferates, and limitations with respect to computational feasibility and accuracy are being reached. It appears therefore natural to abandon PW representations completely and work directly with vector variables, if one wants to calculate 3N scattering at higher energies. As an aside, the use of vector variables is common practice in bound state calculations based on variational [3] and Green's Function Monte Carlo (GFMC) methods [4], which are carried out in coordinate space.

Momentum space calculations within the Faddeev scheme which did not employ a PW decomposition were first carried out for a system of three bosons [5,6]. Here the momentum space Faddeev equations were solved for the bound as well as the scattering state. In this work we want to employ realistic nucleon-nucleon (NN) interactions in a 3N scattering calculation. This means we have to incorporate spin degrees of freedom into the formulation of the Faddeev equations. Since the input to any Faddeev calculation is the solution of the Lippmann-Schwinger (LS) equation for the two-nucleon T-matrix, we start from the formulation of NN scattering developed in Ref. [7]. There we chose an approach based on the total helicity of the NN system as spin variable. From our point of view this is the preferred starting point to later progress to the 3N system.

In this work we consider the first term of the multiple scattering series built up by the Faddeev equations, rather than solve the full Faddeev equations for three nucleons, and concentrate on semi-exclusive break-up observables. Of particular interest are the polarization-transfer coefficients in the (p,n) charge exchange reaction on the deuteron, which recently have been measured at IUCF with a projectile energy of 197 MeV [8] and at RCNP with a projectile energy of 346 MeV [9]. Since these measurements are carried out at 'intermediate energies', one can speculate that it may be sufficient to consider only the first order term in the multiple scattering series. Furthermore, since the projectile energies are high, we will consider relativistic effects as far as the kinematics is concerned.

In Section II we formulate the Nd break-up process in a three-dimensional (3D), nonrelativistic Faddeev scheme. We derive the leading term of the full Nd break-up amplitude, where NN T-matrix elements are given in the momentum-helicity basis defined in Ref. [7]. In Section III we introduce relativistic kinematics into this formulation. We will not consider a boost of the NN T-matrix [10] nor Wigner's rotations [11] of the spin. The observables for

the (p,n) charge exchange reaction are introduced in Section IV. In Section V we present and discuss our calculations for the (p,n) charge exchange reaction in the proton-deuteron (pd) break-up process. Here only the outgoing neutron is detected after the break-up. We present calculations of spin averaged differential cross sections, neutron polarizations, proton analyzing powers, and polarization-transfer coefficients at different energies. We also compare our calculations with traditional PW calculations. Finally, we summarize in Section VI.

II. THE NONRELATIVISTIC ND BREAK-UP AMPLITUDE

In the Faddeev scheme the operator U_0^{full} for the Nd break-up process is given as [2]

$$U_0^{full} = (1 + P)T_F. \quad (2.1)$$

Here T_F is the Faddeev operator obeying the Faddeev equation [1] for the break-up process of three identical particles,

$$T_F = TP + TG_0PT_F. \quad (2.2)$$

The operator T stands for the NN t-matrix, and P is a permutation operator defined as

$$P \equiv P_{12}P_{23} + P_{13}P_{23}. \quad (2.3)$$

The free three-nucleon (3N) propagator is given by G_0 . The matrix elements of the break-up amplitude $U_0^{full}(\mathbf{p}, \mathbf{q})$ of Eq. (2.1) are defined as

$$\begin{aligned} U_0^{full}(\mathbf{p}, \mathbf{q}) &\equiv \left\langle \mathbf{p} \mathbf{q} m_{s1} m_{s2} m_{s3} \tau_1 \tau_2 \tau_3 \middle| U_0^{full} \middle| \mathbf{q}_0 m_{s1}^0 \tau_1^0 \Psi_d^{M_d} \right\rangle \\ &= \left\langle \mathbf{p} \mathbf{q} m_{s1} m_{s2} m_{s3} \tau_1 \tau_2 \tau_3 \middle| (1 + P)T_F \middle| \mathbf{q}_0 m_{s1}^0 \tau_1^0 \Psi_d^{M_d} \right\rangle, \end{aligned} \quad (2.4)$$

where

$$|\mathbf{p} \mathbf{q} m_{s1} m_{s2} m_{s3} \tau_1 \tau_2 \tau_3\rangle \equiv |\mathbf{q} m_{s1} \tau_1\rangle |\mathbf{p} m_{s2} m_{s3} \tau_2 \tau_3\rangle \quad (2.5)$$

is the final, not-antisymmetrized free 3N state. The quantities m_{si}, τ_i ($i = 1, 2, 3$) are the spins and isospins of the three nucleons. The initial state, in which only the deuteron state $|\Psi_d^{M_d}\rangle$ is antisymmetrized, is given by

$$|\mathbf{q}_0 m_{s1}^0 \tau_1^0 \Psi_d^{M_d}\rangle \equiv |\mathbf{q}_0 m_{s1}^0 \tau_1^0\rangle |\Psi_d^{M_d}\rangle \quad (2.6)$$

The index M_d indicates the projection of total angular momentum of the deuteron along an arbitrary z-axis, m_{s1}^0, τ_1^0 are the spin and isospin of nucleon ‘1’ acting as the projectile. Without loss of generality nucleon ‘1’ is singled out as projectile, while the other two nucleons, ‘2’ and ‘3’ form the two-nucleon (2N) subsystem, i.e. the deuteron in the initial state. Jacobi momenta \mathbf{p} and \mathbf{q} are used to describe the 3N kinematics in the final state,

$$\mathbf{p} = \frac{1}{2} (\mathbf{k}_2 - \mathbf{k}_3) \quad (2.7)$$

$$\mathbf{q} = \frac{2}{3} \left[\mathbf{k}_1 - \frac{1}{2} (\mathbf{k}_2 + \mathbf{k}_3) \right] = \mathbf{k}_1 - \frac{1}{3} \mathbf{k}_{lab}. \quad (2.8)$$

Here the \mathbf{k}_i 's ($i = 1, 2, 3$) represent the laboratory momenta of the three nucleons. Defining \mathbf{k}_{lab} as the laboratory momentum of the projectile and applying momentum conservation

$$\mathbf{k}_{lab} = \mathbf{k}_1 + \mathbf{k}_2 + \mathbf{k}_3, \quad (2.9)$$

leads to Eq. (2.8). In the initial state \mathbf{q}_0 is the relative momentum of the projectile to the target deuteron and is related to \mathbf{k}_{lab} as

$$\mathbf{q}_0 = \frac{2}{3} \mathbf{k}_{lab}. \quad (2.10)$$

For clarity of description we will in the following denote the break-up amplitude as $U_0^{full}(\mathbf{p}, \mathbf{q})$ and suppress all other quantum numbers.

In this work we only want to consider the leading term of the full break-up operator U_0^{full} . This means we only consider the leading term in the Faddeev operator T_F of Eq. (2.2) and define the break-up operator U_0 in first order in the NN T-matrix as

$$U_0 = (1 + P)TP. \quad (2.11)$$

The matrix elements of $U_0(\mathbf{p}, \mathbf{q})$ with respect to the final and initial states from Eqs. (2.5) and (2.6) are then given as

$$\begin{aligned} U_0(\mathbf{p}, \mathbf{q}) &\equiv \left\langle \mathbf{p} \mathbf{q} m_{s1} m_{s2} m_{s3} \tau_1 \tau_2 \tau_3 \left| U_0 \right| \mathbf{q}_0 m_{s1}^0 \tau_1^0 \Psi_d^{M_d} \right\rangle \\ &= \left\langle \mathbf{p} \mathbf{q} m_{s1} m_{s2} m_{s3} \tau_1 \tau_2 \tau_3 \left| (1 + P)TP \right| \mathbf{q}_0 m_{s1}^0 \tau_1^0 \Psi_d^{M_d} \right\rangle. \end{aligned} \quad (2.12)$$

From now one we mean by the Nd break-up amplitude (or break-up amplitude) the matrix element $U_0(\mathbf{p}, \mathbf{q})$ given in Eq. (2.12) and by the full Nd break-up amplitude (or full break-up amplitude) the matrix element $U_0^{full}(\mathbf{p}, \mathbf{q})$ given in Eq. (2.4).

The break-up amplitude $U_0(\mathbf{p}, \mathbf{q})$ from Eq. (2.12) is composed out of three terms,

$$U_0(\mathbf{p}, \mathbf{q}) = U_0^{(1)}(\mathbf{p}, \mathbf{q}) + U_0^{(2)}(\mathbf{p}, \mathbf{q}) + U_0^{(3)}(\mathbf{p}, \mathbf{q}), \quad (2.13)$$

with

$$U_0^{(1)}(\mathbf{p}, \mathbf{q}) \equiv {}_1 \left\langle \mathbf{p} \mathbf{q} m_{s1} m_{s2} m_{s3} \tau_1 \tau_2 \tau_3 \left| TP \right| \mathbf{q}_0 m_{s1}^0 \tau_1^0 \Psi_d^{M_d} \right\rangle \quad (2.14)$$

$$U_0^{(2)}(\mathbf{p}, \mathbf{q}) \equiv {}_1 \left\langle \mathbf{p} \mathbf{q} m_{s1} m_{s2} m_{s3} \tau_1 \tau_2 \tau_3 \left| P_{12} P_{23} TP \right| \mathbf{q}_0 m_{s1}^0 \tau_1^0 \Psi_d^{M_d} \right\rangle \quad (2.15)$$

$$U_0^{(3)}(\mathbf{p}, \mathbf{q}) \equiv {}_1 \left\langle \mathbf{p} \mathbf{q} m_{s1} m_{s2} m_{s3} \tau_1 \tau_2 \tau_3 \left| P_{13} P_{23} TP \right| \mathbf{q}_0 m_{s1}^0 \tau_1^0 \Psi_d^{M_d} \right\rangle. \quad (2.16)$$

Here the final free 3N state are labeled '1', meaning that nucleons '2' and '3' form the 2N-subsystem. The spin and isospin quantum numbers must be read in the order 123. Applying the permutation operator $P_{12}P_{23}$ to the final state of $U_0^{(2)}(\mathbf{p}, \mathbf{q})$ given in Eq. (2.15) leads to

$$\begin{aligned}
U_0^{(2)}(\mathbf{p}, \mathbf{q}) &= {}_1 \left\langle P_{23} P_{12} \mathbf{p} \mathbf{q} m_{s1} m_{s2} m_{s3} \tau_1 \tau_2 \tau_3 \left| T P \right| \mathbf{q}_0 m_{s1}^0 \tau_1^0 \Psi_d^{M_d} \right\rangle \\
&= {}_3 \left\langle \mathbf{p} \mathbf{q} m_{s1} m_{s2} m_{s3} \tau_1 \tau_2 \tau_3 \left| T P \right| \mathbf{q}_0 m_{s1}^0 \tau_1^0 \Psi_d^{M_d} \right\rangle.
\end{aligned} \tag{2.17}$$

This is now the final state where nucleons ‘1’ and ‘2’ form the 2N subsystem. Accordingly, the spin and isospin quantum numbers associated with the three nucleons read in the order 312. In order to have the same final states as $U_0^{(1)}(\mathbf{p}, \mathbf{q})$ in Eq. (2.14), we need to transform the final state such that nucleons ‘2’ and ‘3’ form the 2N subsystem. This transformation is achieved by the following relation among the Jacobi momenta [12]

$$\mathbf{p}_1 = -\frac{1}{2} \mathbf{p}_3 - \frac{3}{4} \mathbf{q}_3 \quad \mathbf{q}_1 = \mathbf{p}_3 - \frac{1}{2} \mathbf{q}_3, \tag{2.18}$$

where the labels 1 and 3 indicate the nucleon being singled out. This leads to

$$U_0^{(2)}(\mathbf{p}, \mathbf{q}) = {}_1 \left\langle \left(-\frac{1}{2} \mathbf{p} - \frac{3}{4} \mathbf{q} \right) \left(\mathbf{p} - \frac{1}{2} \mathbf{q} \right) m_{s2} m_{s3} m_{s1} \tau_2 \tau_3 \tau_1 \left| T P \right| \mathbf{q}_0 m_{s1}^0 \tau_1^0 \Psi_d^{M_d} \right\rangle. \tag{2.19}$$

Using another relation between Jacobi momenta [12]

$$\mathbf{p}_1 = -\frac{1}{2} \mathbf{p}_2 + \frac{3}{4} \mathbf{q}_2 \quad \mathbf{q}_1 = -\mathbf{p}_2 - \frac{1}{2} \mathbf{q}_2, \tag{2.20}$$

we can obtain $U_0^{(3)}(\mathbf{p}, \mathbf{q})$ in a similar fashion as

$$U_0^{(3)}(\mathbf{p}, \mathbf{q}) = {}_1 \left\langle \left(-\frac{1}{2} \mathbf{p} + \frac{3}{4} \mathbf{q} \right) \left(-\mathbf{p} - \frac{1}{2} \mathbf{q} \right) m_{s3} m_{s1} m_{s2} \tau_3 \tau_1 \tau_2 \left| T P \right| \mathbf{q}_0 m_{s1}^0 \tau_1^0 \Psi_d^{M_d} \right\rangle. \tag{2.21}$$

Since $U_0^{(2)}(\mathbf{p}, \mathbf{q})$ and $U_0^{(3)}(\mathbf{p}, \mathbf{q})$ differ from $U_0^{(1)}(\mathbf{p}, \mathbf{q})$ only in their variables, it is sufficient to work out an expression only for one of them, which we choose to be $U_0^{(1)}(\mathbf{p}, \mathbf{q})$. For calculating subsequently $U_0^{(2)}(\mathbf{p}, \mathbf{q})$ and $U_0^{(3)}(\mathbf{p}, \mathbf{q})$ one only has to perform the following replacements,

$$\text{for } U_0^{(2)}(\mathbf{p}, \mathbf{q}) : \{\tau, m\}_{\{1,2,3\}} \rightarrow \{\tau, m\}_{\{2,3,1\}} \quad \mathbf{p} \rightarrow -\frac{1}{2} \mathbf{p} - \frac{3}{4} \mathbf{q} \quad \mathbf{q} \rightarrow \mathbf{p} - \frac{1}{2} \mathbf{q} \tag{2.22}$$

$$\text{for } U_0^{(3)}(\mathbf{p}, \mathbf{q}) : \{\tau, m\}_{\{1,2,3\}} \rightarrow \{\tau, m\}_{\{3,1,2\}} \quad \mathbf{p} \rightarrow -\frac{1}{2} \mathbf{p} + \frac{3}{4} \mathbf{q} \quad \mathbf{q} \rightarrow -\mathbf{p} - \frac{1}{2} \mathbf{q}. \tag{2.23}$$

For calculating $U_0^{(1)}(\mathbf{p}, \mathbf{q})$ we start by inserting the following completeness relation for the free 3N system

$$\sum_{\substack{m_{s1} m_{s2} m_{s3} \\ \tau_1 \tau_2 \tau_3}} \int d\mathbf{p} \int d\mathbf{q} |\mathbf{p} \mathbf{q} m_{s1} m_{s2} m_{s3} \tau_1 \tau_2 \tau_3 \rangle \langle \mathbf{p} \mathbf{q} m_{s1} m_{s2} m_{s3} \tau_1 \tau_2 \tau_3| = 1 \tag{2.24}$$

twice into Eq. (2.14), which leads to

$$U_0^{(1)}(\mathbf{p}, \mathbf{q}) = \sum_{\substack{m'_s m'_s m'_s \\ \tau'_1 \tau'_2 \tau'_3}} \int d\mathbf{p}' \int d\mathbf{q}' \langle \mathbf{p} \mathbf{q} m_{s1} m_{s2} m_{s3} \tau_1 \tau_2 \tau_3 | T | \mathbf{p}' \mathbf{q}' m'_s m'_s m'_s \tau'_1 \tau'_2 \tau'_3 \rangle$$

$$\begin{aligned}
& \times \sum_{\substack{m''_{s1} m''_{s2} m''_{s3} \\ \tau''_1 \tau''_2 \tau''_3}} \int d\mathbf{p}'' \int d\mathbf{q}'' \langle \mathbf{p}' \mathbf{q}' m'_{s1} m'_{s2} m'_{s3} \tau'_1 \tau'_2 \tau'_3 | P | \mathbf{p}'' \mathbf{q}'' m''_{s1} m''_{s2} m''_{s3} \tau''_1 \tau''_2 \tau''_3 \rangle \\
& \times \langle \mathbf{p}'' \mathbf{q}'' m''_{s1} m''_{s2} m''_{s3} \tau''_1 \tau''_2 \tau''_3 | \mathbf{q}_0 m^0_{s1} \tau^0_1 \Psi_d^{M_d} \rangle \\
& = \sum_{m'_{s2} m'_{s3} \tau'_2 \tau'_3} \int d\mathbf{p}' \langle \mathbf{p} m_{s2} m_{s3} \tau_2 \tau_3 | T(E_p) | \mathbf{p}' m'_{s2} m'_{s3} \tau'_2 \tau'_3 \rangle \\
& \times \sum_{m''_{s2} m''_{s3} \tau''_2 \tau''_3} \int d\mathbf{p}'' \langle \mathbf{p}' m'_{s2} m'_{s3} \tau'_2 \tau'_3 | \langle \mathbf{q} m_{s1} \tau_1 | P | \mathbf{q}_0 m^0_{s1} \tau^0_1 \rangle | \mathbf{p}'' m''_{s2} m''_{s3} \tau''_2 \tau''_3 \rangle \\
& \times \langle \mathbf{p}'' m''_{s2} m''_{s3} \tau''_2 \tau''_3 | \Psi_d^{M_d} \rangle. \tag{2.25}
\end{aligned}$$

In arriving at the last equality we used the fact that T acts only in the two-particle subsystem together with momentum space properties of the initial state.

The NN T-matrix is calculated at a center of mass (c.m.) energy E_p of the 23-subsystem

$$E_p \equiv \frac{p^2}{m} = \frac{3}{4m}(q_0^2 - q^2) + E_d, \tag{2.26}$$

which does not necessarily corresponds to the intermediate relative momenta \mathbf{p}' . The deuteron binding energy is represented by E_d , and m stand for the nucleon mass.

Using the relations for Jacobi momenta given in Eqs. (2.18) and (2.20) the evaluation of the permutations in Eq. (2.25) leads to

$$\begin{aligned}
& \langle \mathbf{p}' m'_{s2} m'_{s3} \tau'_2 \tau'_3 | \langle \mathbf{q} m_{s1} \tau_1 | P | \mathbf{q}_0 m^0_{s1} \tau^0_1 \rangle | \mathbf{p}'' m''_{s2} m''_{s3} \tau''_2 \tau''_3 \rangle \\
& = {}_1 \langle \mathbf{p}' | \langle \mathbf{q} | \mathbf{q}_0 \rangle | \mathbf{p}'' \rangle_2 {}_1 \left\langle m_{s1} m'_{s2} m'_{s3} \tau_1 \tau'_2 \tau'_3 \left| m^0_{s1} m''_{s2} m''_{s3} \tau^0_1 \tau''_2 \tau''_3 \right. \right\rangle_2 \\
& \quad + {}_1 \langle \mathbf{p}' | \langle \mathbf{q} | \mathbf{q}_0 \rangle | \mathbf{p}'' \rangle_3 {}_1 \left\langle m_{s1} m'_{s2} m'_{s3} \tau_1 \tau'_2 \tau'_3 \left| m^0_{s1} m''_{s2} m''_{s3} \tau^0_1 \tau''_2 \tau''_3 \right. \right\rangle_3 \\
& = {}_1 \left\langle \mathbf{p}' \left| \left\langle \mathbf{q} \right| - \mathbf{p}'' - \frac{1}{2} \mathbf{q}_0 \right\rangle \right| - \frac{1}{2} \mathbf{p}'' + \frac{3}{4} \mathbf{q}_0 \right\rangle_1 {}_1 \left\langle m_{s1} m'_{s2} m'_{s3} \tau_1 \tau'_2 \tau'_3 \left| m''_{s3} m^0_{s1} m''_{s2} \tau''_3 \tau^0_1 \tau''_2 \right. \right\rangle_1 \\
& \quad + {}_1 \left\langle \mathbf{p}' \left| \left\langle \mathbf{q} \right| \mathbf{p}'' - \frac{1}{2} \mathbf{q}_0 \right\rangle \right| - \frac{1}{2} \mathbf{p}'' - \frac{3}{4} \mathbf{q}_0 \right\rangle_1 {}_1 \left\langle m_{s1} m'_{s2} m'_{s3} \tau_1 \tau'_2 \tau'_3 \left| m''_{s2} m''_{s3} m^0_{s1} \tau''_2 \tau''_3 \tau^0_1 \right. \right\rangle_1 \\
& = \delta(\mathbf{p}' - \boldsymbol{\pi}) \delta(\mathbf{p}'' - \boldsymbol{\pi}') \delta_{m_{s1} m''_{s3}} \delta_{m'_{s2} m^0_{s1}} \delta_{m'_{s3} m''_{s2}} \delta_{\tau_1 \tau''_3} \delta_{\tau'_2 \tau^0_1} \delta_{\tau'_3 \tau''_2} \\
& \quad + \delta(\mathbf{p}' + \boldsymbol{\pi}) \delta(\mathbf{p}'' + \boldsymbol{\pi}') \delta_{m_{s1} m''_{s2}} \delta_{m'_{s2} m''_{s3}} \delta_{m'_{s3} m^0_{s1}} \delta_{\tau_1 \tau''_2} \delta_{\tau'_2 \tau''_3} \delta_{\tau'_3 \tau^0_1}, \tag{2.27}
\end{aligned}$$

where

$$\boldsymbol{\pi} \equiv \frac{1}{2} \mathbf{q} + \mathbf{q}_0 \quad \boldsymbol{\pi}' \equiv -\mathbf{q} - \frac{1}{2} \mathbf{q}_0. \tag{2.28}$$

As an aside, the variables are arranged such that each delta function only contains one integration variable. Inserting Eq. (2.27) into $U_0^{(1)}(\mathbf{p}, \mathbf{q})$ in Eq. (2.25) leads to

$$\begin{aligned}
U_0^{(1)}(\mathbf{p}, \mathbf{q}) & = \sum_{m'_{s3} \tau'_3} \langle \mathbf{p} m_{s2} m_{s3} \tau_2 \tau_3 | T(E_p) | \boldsymbol{\pi} m^0_{s1} m'_{s3} \tau^0_1 \tau'_3 \rangle \langle \boldsymbol{\pi}' m'_{s3} m_{s1} \tau'_3 \tau_1 | \Psi_d^{M_d} \rangle \\
& \quad + \sum_{m'_{s2} \tau'_2} \langle \mathbf{p} m_{s2} m_{s3} \tau_2 \tau_3 | T(E_p) | -\boldsymbol{\pi} m'_{s2} m^0_{s1} \tau'_2 \tau^0_1 \rangle \langle -\boldsymbol{\pi}' m_{s1} m'_{s2} \tau_1 \tau'_2 | \Psi_d^{M_d} \rangle
\end{aligned}$$

$$\begin{aligned}
&= \sum_{m'_s \tau'} \left\{ \left\langle \mathbf{p} m_{s2} m_{s3} \tau_2 \tau_3 | T(E_p) | \boldsymbol{\pi} m_{s1}^0 m'_s \tau_1^0 \tau' \right\rangle \left\langle \boldsymbol{\pi}' m'_s m_{s1} \tau' \tau_1 | \Psi_d^{M_d} \right\rangle \right. \\
&\quad \left. + \left\langle \mathbf{p} m_{s2} m_{s3} \tau_2 \tau_3 | T(E_p) P_{23} | \boldsymbol{\pi} m_{s1}^0 m'_s \tau_1^0 \tau' \right\rangle \left\langle \boldsymbol{\pi}' m'_s m_{s1} \tau' \tau_1 | P_{23}^{-1} | \Psi_d^{M_d} \right\rangle \right\} \\
&= \sum_{m'_s \tau'} \left\langle \mathbf{p} m_{s2} m_{s3} \tau_2 \tau_3 | T(E_p)(1 - P_{23}) | \boldsymbol{\pi} m_{s1}^0 m'_s \tau_1^0 \tau' \right\rangle \left\langle \boldsymbol{\pi}' m'_s m_{s1} \tau' \tau_1 | \Psi_d^{M_d} \right\rangle \\
&= \sum_{m'_s \tau'} \left\langle \mathbf{p} m_{s2} m_{s3} \tau_2 \tau_3 | T(E_p) | \boldsymbol{\pi} m_{s1}^0 m'_s \tau_1^0 \tau' \right\rangle_a \left\langle \boldsymbol{\pi}' m'_s m_{s1} \tau' \tau_1 | \Psi_d^{M_d} \right\rangle. \quad (2.29)
\end{aligned}$$

In arriving at the last equality of Eq. (2.29) we made use of the antisymmetry of the deuteron state, $|\Psi_d^{M_d}\rangle$ and defined ${}_a \langle \mathbf{p} m_{s2} m_{s3} \tau_2 \tau_3 | T(E_p) | \boldsymbol{\pi} m_{s1}^0 m'_s \tau_1^0 \tau' \rangle_a$ as

$${}_a \langle \mathbf{p} m_{s2} m_{s3} \tau_2 \tau_3 | T(E_p) | \boldsymbol{\pi} m_{s1}^0 m'_s \tau_1^0 \tau' \rangle_a \equiv \langle \mathbf{p} m_{s2} m_{s3} \tau_2 \tau_3 | T(E_p)(1 - P_{23}) | \boldsymbol{\pi} m_{s1}^0 m'_s \tau_1^0 \tau' \rangle. \quad (2.30)$$

We denote the matrix element ${}_a \langle \mathbf{p} m_{s2} m_{s3} \tau_2 \tau_3 | T(E_p) | \boldsymbol{\pi} m_{s1}^0 m'_s \tau_1^0 \tau' \rangle_a$ as physical representation of the NN T-matrix, physical meaning that the NN basis states $|\mathbf{p} m_{s2} m_{s3} \tau_2 \tau_3\rangle_a$ contain the individual spins and isospins of the nucleons.

Since the deuteron contains only two definite angular momentum states, it is reasonable to apply the standard partial wave expansion

$$\begin{aligned}
|\Psi_d^{M_d}\rangle &= \sum_{lsjm} \int dp' p'^2 |p'(ls)jm; t\rangle \langle p'(ls)jm; t | \Psi_d^{M_d}\rangle \\
&= \sum_l \int dp' p'^2 |p'(l1)1M_d; 0\rangle \psi_l(p'). \quad (2.31)
\end{aligned}$$

Here $|p'(ls)jm; t\rangle$ is the standard partial wave basis, and $\psi_l(p')$ represent the standard s - and d -waves of the deuteron. The projection $\langle \boldsymbol{\pi}' m'_s m_{s1} \tau' \tau_1 | \Psi_d^{M_d} \rangle$ on the deuteron state in Eq. (2.29) is then explicitly worked out as

$$\begin{aligned}
\langle \boldsymbol{\pi}' m'_s m_{s1} \tau' \tau_1 | \Psi_d^{M_d} \rangle &= \sum_l \int dp' p'^2 \langle \boldsymbol{\pi}' m'_s m_{s1} \tau' \tau_1 | p'(l1)1M_d; 0 \rangle \psi_l(p') \\
&= \langle \tau' \tau_1 | 0 \rangle \sum_{l\mu} C(l11; \mu, M_d - \mu) \\
&\quad \times \int dp' p'^2 \langle \boldsymbol{\pi}' | p' l \mu \rangle \langle m'_s m_{s1} | 1, M_d - \mu \rangle \psi_l(p') \\
&= C\left(\frac{1}{2} \frac{1}{2} 0; \tau' \tau_1\right) \sum_{l\mu} C(l11; \mu, M_d - \mu) \\
&\quad \times Y_{l\mu}(\hat{\boldsymbol{\pi}}') C\left(\frac{1}{2} \frac{1}{2} 1; m'_s m_{s1}\right) \delta_{m'_s + m_{s1}, M_d - \mu} \psi_l(\pi') \\
&= C\left(\frac{1}{2} \frac{1}{2} 0; \tau' \tau_1\right) C\left(\frac{1}{2} \frac{1}{2} 1; m'_s m_{s1}\right) \\
&\quad \times \sum_l C(l11; M_d - m'_s - m_{s1}, m'_s + m_{s1}) \\
&\quad \times Y_{l, M_d - m'_s - m_{s1}}(\hat{\boldsymbol{\pi}}') \psi_l(\pi'). \quad (2.32)
\end{aligned}$$

Finally, inserting Eq. (2.32) into Eq. (2.29) we obtain the first part of the break-up amplitude $U_0^{(1)}(\mathbf{p}, \mathbf{q})$ as

$$\begin{aligned}
U_0^{(1)}(\mathbf{p}, \mathbf{q}) &= \sum_{m'_s \tau'} \langle \mathbf{p} m_{s2} m_{s3} \tau_2 \tau_3 | T(E_p) | \boldsymbol{\pi} m_{s1}^0 m'_s \tau_1^0 \tau' \rangle_a C\left(\frac{1}{2} \frac{1}{2} 0; \tau' \tau_1\right) C\left(\frac{1}{2} \frac{1}{2} 1; m'_s m_{s1}\right) \\
&\quad \times \sum_l C(l11; M_d - m'_s - m_{s1}, m'_s + m_{s1}) Y_{l, M_d - m'_s - m_{s1}}(\hat{\boldsymbol{\pi}}') \psi_l(\pi') \\
&= \frac{(-)^{\frac{1}{2} + \tau_1}}{\sqrt{2}} \sum_{m'_s} C\left(\frac{1}{2} \frac{1}{2} 1; m'_s m_{s1}\right) \langle \mathbf{p} m_{s2} m_{s3} \tau_2 \tau_3 | T(E_p) | \boldsymbol{\pi} m_{s1}^0 m'_s \tau_1^0 \tau' \rangle_a \\
&\quad \times \sum_l C(l11; M_d - m'_s - m_{s1}, m'_s + m_{s1}) Y_{l, M_d - m'_s - m_{s1}}(\hat{\boldsymbol{\pi}}') \psi_l(\pi'). \tag{2.33}
\end{aligned}$$

Eq. (2.33) may serve as a starting point for further expressions for $U_0^{(1)}(\mathbf{p}, \mathbf{q})$ to be used in the explicit calculations. It shows how $U_0^{(1)}(\mathbf{p}, \mathbf{q})$ depends on the PW projected components of the deuteron and on the NN T-matrix in a physical representation. In our calculation of the Nd break-up process we employ the NN t-matrix in the momentum-helicity basis $|\mathbf{p}; \hat{\mathbf{p}} S \Lambda; t\rangle^{\pi a}$ [7], where S , t , Λ are the total spin of the 2N system, the total isospin and the helicity. The label πa means that the basis state has a definite parity η_π and is antisymmetrized. The connection of the T-matrix elements $\langle \mathbf{p} m_{s2} m_{s3} \tau_2 \tau_3 | T(E_p) | \boldsymbol{\pi} m_{s1}^0 m'_s \tau_1^0 \tau' \rangle_a$ to those in the momentum-helicity basis, namely $T_{\Lambda \Lambda'}^{\pi S t}(\mathbf{p}, \boldsymbol{\pi}; E_p)$, is given in Ref. [7]. Here we want to be more general by letting the nucleon types τ_2 , τ_3 , τ_1^0 , τ_1 being arbitrary but employing Kronecker symbols to ensure charge conservation,

$$\begin{aligned}
a \langle \tau_2 \tau_3 m_{s2} m_{s3} \mathbf{p} | T(E_p) | \tau_1^0, -\tau_1 m_{s1}^0 m'_s \boldsymbol{\pi} \rangle_a &= \frac{1}{4} \delta_{\tau_2 + \tau_3, \tau_1^0 - \tau_1} e^{-i(\Lambda_0 \phi_p - \Lambda'_0 \phi_\pi)} \sum_{S \pi t} (1 - \eta_\pi(-)^{S+t}) C\left(\frac{1}{2} \frac{1}{2} t; \tau_2 \tau_3\right) C\left(\frac{1}{2} \frac{1}{2} t; \tau_1^0, -\tau_1\right) \\
&\quad \times C\left(\frac{1}{2} \frac{1}{2} S; m_{s2} m_{s3} \Lambda_0\right) C\left(\frac{1}{2} \frac{1}{2} S; m_{s1}^0 m'_s \Lambda'_0\right) \\
&\quad \times \sum_{\Lambda \Lambda'} d_{\Lambda_0 \Lambda}^S(\theta_p) d_{\Lambda'_0 \Lambda'}^S(\theta_\pi) T_{\Lambda \Lambda'}^{\pi S t}(\mathbf{p}, \boldsymbol{\pi}; E_p). \tag{2.34}
\end{aligned}$$

In the above expression $d_{\Lambda' \Lambda}^S(\theta)$ is a rotation matrix [13]. Using Eq. (2.34) we obtain $U_0^{(1)}(\mathbf{p}, \mathbf{q})$ in terms of the NN T-matrix elements $T_{\Lambda \Lambda'}^{\pi S t}(\mathbf{p}, \boldsymbol{\pi}; E_p)$ in the momentum-helicity basis as

$$\begin{aligned}
U_0^{(1)}(\mathbf{p}, \mathbf{q}) &= \frac{(-)^{\frac{1}{2} + \tau_1}}{4\sqrt{2}} \delta_{\tau_2 + \tau_3, \tau_1^0 - \tau_1} \sum_{m'_s} e^{-i(\Lambda_0 \phi_p - \Lambda'_0 \phi_\pi)} C\left(\frac{1}{2} \frac{1}{2} 1; m'_s m_{s1}\right) \\
&\quad \times \sum_l C(l11; M_d - m'_s - m_{s1}, m'_s + m_{s1}) Y_{l, M_d - m'_s - m_{s1}}(\hat{\boldsymbol{\pi}}') \psi_l(\pi') \\
&\quad \times \sum_{S \pi t} (1 - \eta_\pi(-)^{S+t}) C\left(\frac{1}{2} \frac{1}{2} t; \tau_2 \tau_3\right) C\left(\frac{1}{2} \frac{1}{2} t; \tau_1^0, -\tau_1\right) \\
&\quad \times C\left(\frac{1}{2} \frac{1}{2} S; m_{s2} m_{s3} \Lambda_0\right) C\left(\frac{1}{2} \frac{1}{2} S; m_{s1}^0 m'_s \Lambda'_0\right) \\
&\quad \times \sum_{\Lambda \Lambda'} d_{\Lambda_0 \Lambda}^S(\theta_p) d_{\Lambda'_0 \Lambda'}^S(\theta_\pi) T_{\Lambda \Lambda'}^{\pi S t}(\mathbf{p}, \boldsymbol{\pi}; E_p). \tag{2.35}
\end{aligned}$$

Now let us concentrate on the NN T-matrix elements $T_{\Lambda\Lambda'}^{\pi St}(\mathbf{p}, \mathbf{p}'; E_p)$ in the momentum-helicity basis. For the calculation of NN scattering it is convenient to choose the z-axis as the direction of the initial momenta \mathbf{p}' . It is shown in Ref. [7] that in this case the azimuthal dependencies of the T-matrix elements can be separated as

$$T_{\Lambda\Lambda'}^{\pi St}(\mathbf{p}, p'\hat{\mathbf{z}}; E_p) = e^{i\Lambda'\phi} T_{\Lambda\Lambda'}^{\pi St}(p, p', \cos\theta; E_p), \quad (2.36)$$

which then allowed to reduce the LSE's for $T_{\Lambda\Lambda'}^{\pi St}(\mathbf{p}, p'\hat{\mathbf{z}}; E_p)$ to be the ones for $T_{\Lambda\Lambda'}^{\pi St}(p, p', \cos\theta; E_p)$. Thus, in order to calculate $U_0^{(1)}(\mathbf{p}, \mathbf{q})$ we have to find a relation between $T_{\Lambda\Lambda'}^{\pi St}(\mathbf{p}, \mathbf{p}'; E_p)$ with arbitrary $\hat{\mathbf{p}}'$ and $T_{\Lambda\Lambda'}^{\pi St}(p, p', \cos\theta''; E_p)$, where θ'' now depends on $\hat{\mathbf{p}}$ and $\hat{\mathbf{p}}'$. This is done in the following way. First we rotate $T_{\Lambda\Lambda'}^{\pi St}(\mathbf{p}, \mathbf{p}'; E_p)$ so that $\hat{\mathbf{p}}'$ points in the z-direction and then apply the relation given in Eq. (2.36). With $R(\hat{\mathbf{p}}')$ being a rotation operator working in momentum and spin space, it follows according to Ref. [7] that

$$\begin{aligned} T_{\Lambda\Lambda'}^{\pi St}(\mathbf{p}, \mathbf{p}'; E_p) &= {}^{\pi a} \langle \mathbf{p}; \hat{\mathbf{p}} S\Lambda; t | T(E_p) | \mathbf{p}'; \hat{\mathbf{p}}' S\Lambda'; t \rangle^{\pi a} \\ &= {}^{\pi a} \langle \mathbf{p}; \hat{\mathbf{p}} S\Lambda; t | T(E_p) R(\hat{\mathbf{p}}') | p'\hat{\mathbf{z}}; \hat{\mathbf{z}} S\Lambda'; t \rangle^{\pi a} \\ &= {}^{\pi a} \langle \mathbf{p}; \hat{\mathbf{p}} S\Lambda; t | R(\hat{\mathbf{p}}') T(E_p) | p'\hat{\mathbf{z}}; \hat{\mathbf{z}} S\Lambda'; t \rangle^{\pi a} \\ &= {}^{\pi a} \langle R^\dagger(\hat{\mathbf{p}}') \mathbf{p}; \hat{\mathbf{p}} S\Lambda; t | T(E_p) | p'\hat{\mathbf{z}}; \hat{\mathbf{z}} S\Lambda'; t \rangle^{\pi a}. \end{aligned} \quad (2.37)$$

Here

$$|\mathbf{p}; \hat{\mathbf{p}} S\Lambda; t\rangle^{\pi a} \equiv \frac{1}{2} (1 - \eta_\pi(-)^{S+t}) (1 + \eta_\pi) |t\rangle |\mathbf{p}; \hat{\mathbf{p}} S\Lambda\rangle, \quad (2.38)$$

and thus,

$$R^\dagger(\hat{\mathbf{p}}') |\mathbf{p}; \hat{\mathbf{p}} S\Lambda; t\rangle^{\pi a} = \frac{1}{2} (1 - \eta_\pi(-)^{S+t}) (1 + \eta_\pi) |t\rangle R^\dagger(\hat{\mathbf{p}}') |\mathbf{p}; \hat{\mathbf{p}} S\Lambda\rangle. \quad (2.39)$$

The action of $R^\dagger(\hat{\mathbf{p}}')$ on the state $|\mathbf{p}; \hat{\mathbf{p}} S\Lambda\rangle$ leads to two successive rotations as

$$R^\dagger(\hat{\mathbf{p}}') |\mathbf{p}; \hat{\mathbf{p}} S\Lambda\rangle = R(0, -\theta', -\phi') R(\phi\theta0) |p\hat{\mathbf{z}}; \hat{\mathbf{z}} S\Lambda\rangle, \quad (2.40)$$

and the result is (see Appendix A for the derivation) given by

$$\begin{aligned} R^\dagger(\hat{\mathbf{p}}') |\mathbf{p}; \hat{\mathbf{p}} S\Lambda\rangle &= e^{i\Lambda\Omega} R(\phi''\theta''0) |p\hat{\mathbf{z}}; \hat{\mathbf{z}} S\Lambda\rangle \\ &= e^{i\Lambda\Omega} |\mathbf{p}''; \hat{\mathbf{p}}'' S\Lambda\rangle, \end{aligned} \quad (2.41)$$

with

$$\cos\theta'' = \cos\theta \cos\theta' + \sin\theta \sin\theta' \cos(\phi - \phi') \quad (2.42)$$

$$\sin\theta'' e^{i\phi''} = -\cos\theta \sin\theta' + \sin\theta \cos\theta' \cos(\phi - \phi') + i \sin\theta \sin(\phi - \phi') \quad (2.43)$$

$$e^{i\Lambda\Omega} = \frac{\sum_{N=-S}^S D_{N\Lambda'}^{S*}(\phi'\theta'0) D_{N\Lambda}^S(\phi\theta0)}{D_{\Lambda'\Lambda}^S(\phi''\theta''0)}, \quad (2.44)$$

where $D_{\Lambda'\Lambda}^S(\phi\theta0)$ are the Wigner D-function [13]. Inserting Eq. (2.41) and then Eq. (2.36) into Eq. (2.37) yields

$$\begin{aligned}
T_{\Lambda\Lambda'}^{\pi St}(\mathbf{p}, \mathbf{p}'; E_p) &= e^{-i\Lambda\Omega - \pi a} \langle \mathbf{p}''; \hat{\mathbf{p}}'' S\Lambda; t | T(E_p) | p' \hat{\mathbf{z}}; \hat{\mathbf{z}} S\Lambda'; t \rangle^{\pi a} \\
&= e^{-i\Lambda\Omega} T_{\Lambda\Lambda'}^{\pi St}(\mathbf{p}'', p' \hat{\mathbf{z}}; E_p) \\
&= e^{i(\Lambda'\phi'' - \Lambda\Omega)} T_{\Lambda\Lambda'}^{\pi St}(p, p', \cos\theta''; E_p),
\end{aligned} \tag{2.45}$$

where the exponential factor $e^{i(\Lambda'\phi'' - \Lambda\Omega)}$ is calculated as

$$\begin{aligned}
e^{i(\Lambda'\phi'' - \Lambda\Omega)} &= e^{i\Lambda'\phi''} \frac{\sum_{N=-S}^S D_{N\Lambda}^{S*}(\phi\theta 0) D_{N\Lambda'}^S(\phi'\theta' 0)}{D_{\Lambda'\Lambda}^{S*}(\phi''\theta'' 0)} \\
&= \frac{\sum_{N=-S}^S e^{iN(\phi-\phi')} d_{N\Lambda}^S(\theta) d_{N\Lambda'}^S(\theta')}{d_{\Lambda'\Lambda}^S(\theta'')}.
\end{aligned} \tag{2.46}$$

Returning to Eq. (2.35), by means of the relation given in Eq. (2.45) we arrive at our final expression for $U_0^{(1)}(\mathbf{p}, \mathbf{q})$:

$$\begin{aligned}
U_0^{(1)}(\mathbf{p}, \mathbf{q}) &= \frac{(-)^{\frac{1}{2}+\tau_1}}{4\sqrt{2}} \delta_{\tau_2+\tau_3, \tau_1^0-\tau_1} \sum_{m'_s} e^{-i(\Lambda_0\phi_p - \Lambda'_0\phi_\pi)} C\left(\frac{1}{2} \frac{1}{2} 1; m'_s m_{s1}\right) \\
&\quad \times \sum_l C(l11; M_d - m'_s - m_{s1}, m'_s + m_{s1}) Y_{l, M_d - m'_s - m_{s1}}(\hat{\boldsymbol{\pi}}') \psi_l(\pi') \\
&\quad \times \sum_{S\pi t} (1 - \eta_\pi(-)^{S+t}) C\left(\frac{1}{2} \frac{1}{2} t; \tau_2 \tau_3\right) C\left(\frac{1}{2} \frac{1}{2} t; \tau_1^0, -\tau_1\right) \\
&\quad \times C\left(\frac{1}{2} \frac{1}{2} S; m_{s2} m_{s3} \Lambda_0\right) C\left(\frac{1}{2} \frac{1}{2} S; m_{s1}^0 m'_s \Lambda'_0\right) \\
&\quad \times \sum_{\Lambda\Lambda'} d_{\Lambda_0\Lambda}^S(\theta_p) d_{\Lambda'_0\Lambda'}^S(\theta_\pi) e^{i(\Lambda'\phi' - \Lambda\Omega)} T_{\Lambda\Lambda'}^{\pi St}(p, \pi, \cos\theta'; E_p),
\end{aligned} \tag{2.47}$$

with

$$\cos\theta' = \cos\theta_p \cos\theta_\pi + \sin\theta_p \sin\theta_\pi \cos(\phi_p - \phi_\pi) \tag{2.48}$$

$$e^{i(\Lambda'\phi' - \Lambda\Omega)} = \frac{\sum_{N=-S}^S e^{iN(\phi_p - \phi_\pi)} d_{N\Lambda}^S(\theta_p) d_{N\Lambda'}^S(\theta_\pi)}{d_{\Lambda'\Lambda}^S(\theta')} \tag{2.49}$$

III. RELATIVISTIC KINEMATICS IN THE ND BREAK-UP AMPLITUDE

In the previous section the break-up operator $U_0(\mathbf{p}, \mathbf{q})$ is derived within the framework of the nonrelativistic Faddeev theory. Since our goal is to study break-up reactions at intermediate energies, we want to consider the influence of relativistic kinematics. This means, that we not only have to employ relativistic energy-momentum relations, but more importantly have to reevaluate the Jacobi momenta, carry out corresponding Lorentz transformations to the two- and three-particle c.m. subsystems, and employ a relativistic description of the cross section. For our derivation we adopt the formulation given in Ref. [14]. For clarity we will describe the most important steps in detail.

A. Jacobi Momenta

Let a system be described by the energy and momentum vector (E, \mathbf{k}) in one frame. Then, in a different frame moving with relative velocity \mathbf{u} , the system is described by (E', \mathbf{k}') , connected by a Lorentz transformation $L(\mathbf{u})$ to the first frame,

$$(E', \mathbf{k}') \equiv L(\mathbf{u})(E, \mathbf{k}) \quad (3.1)$$

$$\mathbf{k}' = \mathbf{k} + (\gamma - 1)(\mathbf{k} \cdot \hat{\mathbf{u}})\hat{\mathbf{u}} - \gamma E \mathbf{u} \quad (3.2)$$

$$E' = \gamma(E - \mathbf{k} \cdot \mathbf{u}) \quad (3.3)$$

$$\gamma \equiv \frac{1}{\sqrt{1 - u^2}}. \quad (3.4)$$

Using these relations we can bring our 3N system from the laboratory frame to the c.m. frame and find the corresponding Jacobi momenta \mathbf{p} and \mathbf{q} in the final state and \mathbf{q}_0 in the initial state.

As in the previous section we choose without loss of generality the two-nucleon subsystem to consist of nucleons 2 and 3, and let nucleon 1 be the spectator. To derive the relative momentum \mathbf{p} of the subsystem in its c.m. frame, we employ the Lorentz transformation

$$\mathbf{u} = \frac{\mathbf{k}_{23}}{E_{23}} \quad (3.5)$$

$$(E'_2, \mathbf{p}) \equiv (E'_2, \mathbf{k}'_2) = L(\mathbf{u})(E_2, \mathbf{k}_2) \quad (3.6)$$

$$(E'_2, -\mathbf{p}) \equiv (E'_3, \mathbf{k}'_3) = L(\mathbf{u})(E_3, \mathbf{k}_3). \quad (3.7)$$

Let us define the following quantities for the 23-subsystem,

$$\mathbf{k}_{23} \equiv \mathbf{k}_2 + \mathbf{k}_3 \quad (3.8)$$

$$E_{23} \equiv E_2 + E_3, \quad (3.9)$$

which are connected by a Lorentz invariant relation as

$$E_{23}^2 - \mathbf{k}_{23}^2 \equiv M_{23}^2 \geq 4m^2. \quad (3.10)$$

Here M_{23} is called the invariant mass of the 23-subsystem and equals the total energy of the 23-subsystem in its c.m. frame. According to Eq. (3.2) and the transformations given in Eqs. (3.5)-(3.7), the Jacobi momentum \mathbf{p} is given as [15]

$$\mathbf{p} = \frac{1}{2}(\mathbf{k}_2 - \mathbf{k}_3) - \frac{1}{2}\mathbf{k}_{23} \left(\frac{E_2 - E_3}{E_{23} + M_{23}} \right). \quad (3.11)$$

The last term in Eq. (3.11) exhibits the relativistic effect in the definition of the relative momentum. Since in the c.m. frame the energy E'_2 is equal to E'_3 , the total energy M_{23} in the 23-frame is given as

$$M_{23} = E'_2 + E'_3 = 2E'_2 = 2\sqrt{m^2 + k'_2} = 2\sqrt{m^2 + p^2}. \quad (3.12)$$

Starting with Eq. (3.12), employing energy and momentum conservation together with Eqs. (3.8)-(3.10) the magnitude of \mathbf{p} is calculated as

$$p = \frac{1}{2} \sqrt{m_d^2 - 2m^2 + 2m_d(E_{lab} - E_1) - 2E_{lab}E_1 + 2k_{lab}k_1 \cos \theta_{lab}}. \quad (3.13)$$

Knowing the total energy M_{23} in the 23-frame one can calculate the kinetic energy E_p in the 23-subsystem, that is

$$E_p = M_{23} - 2m = 2\sqrt{m^2 + p^2} - 2m. \quad (3.14)$$

Thus the NN T-matrix elements $T_{\Lambda\Lambda'}^{\pi St}(p, \pi, \cos \theta'; E_p)$ in Eq. (2.47) will be calculated for the energy E_p given in Eq. (3.14).

In order to obtain the Jacobi momentum \mathbf{q} we apply the following Lorentz transformation

$$\mathbf{u} = \frac{\mathbf{k}_{lab}}{E_0} \quad (3.15)$$

$$(E'_1, \mathbf{q}) \equiv (E'_1, \mathbf{k}'_1) = L(\mathbf{u})(E_1, \mathbf{k}_1) \quad (3.16)$$

$$(E'_{23}, -\mathbf{q}) \equiv (E'_{23}, \mathbf{k}'_{23}) = L(\mathbf{u})(E_{23}, \mathbf{k}_{23}), \quad (3.17)$$

where E_0 is the total energy in the laboratory frame,

$$E_0 \equiv m_d + E_{lab} = E_1 + E_{23}. \quad (3.18)$$

Similar to \mathbf{p} , the Jacobi momentum \mathbf{q} acquires a relativistic correction term and is given by

$$\mathbf{q} = \frac{1}{2}(\mathbf{k}_1 - \mathbf{k}_{23}) + \frac{\mathbf{k}_{lab}}{2M_0} \left(\frac{(\mathbf{k}_1 - \mathbf{k}_{23}) \cdot \mathbf{k}_{lab}}{E_0 + M_0} - (E_1 - E_{23}) \right). \quad (3.19)$$

Here M_0 is c.m. total energy or the invariant mass of the 3N system

$$M_0 \equiv E'_1 + E'_{23}, \quad (3.20)$$

which is connected to the laboratory total energy E_0 and the laboratory total momentum \mathbf{k}_{lab} by the following Lorentz invariant relation

$$E_0^2 - \mathbf{k}_{lab}^2 = M_0^2 \geq 9m^2. \quad (3.21)$$

The energies E'_1 and E'_{23} are given in terms of the magnitudes of Jacobi momenta \mathbf{p} and \mathbf{q} as

$$E'_1 = \sqrt{m^2 + k'_1{}^2} = \sqrt{m^2 + q^2} \quad (3.22)$$

$$E'_{23} = \sqrt{M_{23}^2 + k'_{23}{}^2} = \sqrt{4(m^2 + p^2) + q^2}. \quad (3.23)$$

With Eqs. (3.16)-(3.18), (3.20) and (3.22)-(3.23) we get for the scalar product in Eq. (3.19)

$$\begin{aligned} (\mathbf{k}_1 - \mathbf{k}_{23}) \cdot \mathbf{k}_{lab} &= k_1^2 - k_{23}^2 \\ &= E_1^2 - E_{23}^2 - m^2 + M_{23}^2 \\ &= (E_1 - E_{23})E_0 - (E_1^2 - E_{23}^2) \\ &= (E_1 - E_{23})E_0 - (E'_1 - E'_{23})M_0. \end{aligned} \quad (3.24)$$

Inserting this result into Eq. (3.19) leads to a final expression for \mathbf{q} ,

$$\begin{aligned}
\mathbf{q} &= \frac{1}{2}(\mathbf{k}_1 - \mathbf{k}_{23}) + \frac{\mathbf{k}_{lab}}{2M_0} \left(\frac{(E_1 - E_{23})E_0 - (E'_1 - E'_{23})M_0}{E_0 + M_0} - (E_1 - E_{23}) \right) \\
&= \frac{1}{2}(\mathbf{k}_1 - \mathbf{k}_{23}) - \frac{1}{2}\mathbf{k}_{lab} \left(\frac{E_1 - E_{23} + E'_1 - E'_{23}}{E_0 + M_0} \right) \\
&= \mathbf{k}_1 - \mathbf{k}_{lab} \left(\frac{E_1 + E'_1}{E_0 + M_0} \right).
\end{aligned} \tag{3.25}$$

For the last equality total momentum conservation was employed. With the help of Eqs. (3.22) and (3.23) we can write M_0 as

$$M_0 = E'_1 + E'_{23} = \sqrt{m^2 + q^2} + \sqrt{4(m^2 + p^2) + q^2}. \tag{3.26}$$

Starting from Eq. (3.26) we obtain after some algebra the magnitude of \mathbf{q} as

$$q = \frac{1}{2M_0} \sqrt{\{M_0^2 - (5m^2 + 4p^2)\}^2 - 16m^2(m^2 + p^2)}, \tag{3.27}$$

where the value of M_0 can be calculated from Eq. (3.21) as

$$M_0 = \sqrt{E_0^2 - k_{lab}^2} = \sqrt{m^2 + m_d^2 + 2m_d E_{lab}}. \tag{3.28}$$

Finally we turn to the initial state, calculate the Jacobi momentum \mathbf{q}_0 , the energies E'_{lab} of the incoming nucleon and E'_d of the deuteron in the c.m. frame. Replacing in Eq. (3.19) the quantities \mathbf{k}_1 with \mathbf{k}_{lab} , E_1 with E_{lab} , \mathbf{k}_{23} with zero and E_{23} with m_d , the Jacobi momentum \mathbf{q}_0 is given as

$$\begin{aligned}
\mathbf{q}_0 &= \frac{1}{2}\mathbf{k}_{lab} + \frac{\mathbf{k}_{lab}}{2M_0} \left(\frac{k_{lab}^2}{E_0 + M_0} - (E_{lab} - m_d) \right) \\
&= \frac{1}{2}\mathbf{k}_{lab} + \frac{\mathbf{k}_{lab}}{2M_0} (E_0 - M_0 - (E_{lab} - m_d)) \\
&= \frac{m_d}{M_0} \mathbf{k}_{lab}.
\end{aligned} \tag{3.29}$$

The energies E'_{lab} and E'_d are obtained using Eq. (3.3) as

$$E'_{lab} = \frac{E_0}{M_0} \left(E_{lab} - \frac{k_{lab}^2}{E_0} \right) = \frac{1}{M_0} (m^2 + m_d E_{lab}) \tag{3.30}$$

$$E'_d = \frac{E_0}{M_0} m_d = \frac{1}{M_0} (E_{lab} + m_d) m_d. \tag{3.31}$$

It can be shown that E'_{lab} and E'_d sum up to M_0 as required by total energy conservation in the c.m. frame.

B. S-Matrix

For a correct treatment of relativistic kinematics, we still need to connect the S-matrix element in the laboratory frame to the Nd break-up amplitude. Suppressing all discrete quantum numbers we define the S-matrix element for the break-up process in the laboratory frame as

$$S(\mathbf{k}_1, \mathbf{k}_2, \mathbf{k}_3) \equiv \langle \mathbf{k}_1 \mathbf{k}_2 \mathbf{k}_3 | S | \mathbf{k}_{lab} \mathbf{k}_d \rangle \quad (3.32)$$

and in the c.m. frame as

$$S(\mathbf{p}, \mathbf{q}) \equiv \langle \mathbf{p} \mathbf{q} | S | \mathbf{q}_0 \rangle \equiv \langle \mathbf{p} \mathbf{q} | S | \mathbf{q}_0 \rangle. \quad (3.33)$$

In the above equation we omitted the deuteron state $|\Psi_d\rangle$ in the initial state, but showed its momentum \mathbf{k}_d in Eq. (3.32), though its value is zero. The momenta \mathbf{p} , \mathbf{q} , and \mathbf{q}_0 are the Jacobi momenta calculated in Eqs. (3.11), (3.25), and (3.29). The states $|\mathbf{k}_1 \mathbf{k}_2 \mathbf{k}_3\rangle$ and $|\mathbf{k}_{lab} \mathbf{k}_d\rangle$ are related to the states $|\mathbf{p} \mathbf{q}\rangle$ and $|\mathbf{q}_0\rangle$ by the following relations,

$$\begin{aligned} |\mathbf{k}_1 \mathbf{k}_2 \mathbf{k}_3\rangle &\equiv |\mathbf{k}_1\rangle |\mathbf{k}_2 \mathbf{k}_3\rangle \\ &= J^{-\frac{1}{2}}(\mathbf{k}_2, \mathbf{k}_3) |\mathbf{k}_1\rangle |\mathbf{p} \mathbf{k}_{23}\rangle \\ &\equiv J^{-\frac{1}{2}}(\mathbf{k}_2, \mathbf{k}_3) J^{-\frac{1}{2}}(\mathbf{k}_1, \mathbf{k}_{23}) |\mathbf{p} \mathbf{q}\rangle |\mathbf{k}_1 + \mathbf{k}_{23}\rangle \end{aligned} \quad (3.34)$$

$$|\mathbf{k}_{lab} \mathbf{k}_d\rangle \equiv J^{-\frac{1}{2}}(\mathbf{k}_{lab}, \mathbf{k}_d) |\mathbf{q}_0\rangle |\mathbf{k}_{lab}\rangle. \quad (3.35)$$

The Jacobian $J(\mathbf{k}_2, \mathbf{k}_3)$ of the transformation from the variables $(\mathbf{k}_2, \mathbf{k}_3)$ to $(\mathbf{p}, \mathbf{k}_{23})$ is given by [14]

$$J(\mathbf{k}_2, \mathbf{k}_3) = \left| \frac{\partial(\mathbf{k}_2, \mathbf{k}_3)}{\partial(\mathbf{p}, \mathbf{k}_{23})} \right| = \frac{E_2 E_3}{E_{23}} \frac{M_{23}}{E'_2 E'_3} = \frac{4 E_2 E_3}{E_{23} M_{23}}, \quad (3.36)$$

where the last equality results by means of Eq. (3.12) for M_{23} . Similarly, the Jacobians $J(\mathbf{k}_1, \mathbf{k}_{23})$ in Eq. (3.34) and $J(\mathbf{k}_{lab}, \mathbf{k}_d)$ in Eq. (3.35) are given as

$$J(\mathbf{k}_1, \mathbf{k}_{23}) = \left| \frac{\partial(\mathbf{k}_1, \mathbf{k}_{23})}{\partial(\mathbf{q}, \mathbf{k}_1 + \mathbf{k}_{23})} \right| = \frac{E_1 E_{23}}{E_0} \frac{M_0}{E'_1 E'_{23}} \quad (3.37)$$

$$J(\mathbf{k}_{lab}, \mathbf{k}_d) = \left| \frac{\partial(\mathbf{k}_{lab}, \mathbf{k}_d)}{\partial(\mathbf{q}_0, \mathbf{k}_{lab})} \right| = \frac{E_{lab} m_d}{E_0} \frac{M_0}{E'_{lab} E'_d}. \quad (3.38)$$

Thus, one can finally relate $S(\mathbf{k}_1, \mathbf{k}_2, \mathbf{k}_3)$ to $S(\mathbf{p}, \mathbf{q})$ as

$$\begin{aligned} S(\mathbf{k}_1, \mathbf{k}_2, \mathbf{k}_3) &= \langle \mathbf{k}_1 \mathbf{k}_2 \mathbf{k}_3 | S | \mathbf{k}_{lab} \mathbf{k}_d \rangle \\ &= J^{-\frac{1}{2}}(\mathbf{k}_2, \mathbf{k}_3) J^{-\frac{1}{2}}(\mathbf{k}_1, \mathbf{k}_{23}) J^{-\frac{1}{2}}(\mathbf{k}_{lab}, \mathbf{k}_d) \langle \mathbf{k}_1 + \mathbf{k}_{23} | \langle \mathbf{p} \mathbf{q} | S | \mathbf{q}_0 \rangle | \mathbf{k}_{lab} \rangle \\ &= \delta(\mathbf{k}_1 + \mathbf{k}_{23} - \mathbf{k}_{lab}) \{ J(\mathbf{k}_2, \mathbf{k}_3) J(\mathbf{k}_1, \mathbf{k}_{23}) J(\mathbf{k}_{lab}, \mathbf{k}_d) \}^{-\frac{1}{2}} S(\mathbf{p}, \mathbf{q}), \end{aligned} \quad (3.39)$$

where the delta function ensures total momentum conservation.

As last step we need to connect $S(\mathbf{k}_1, \mathbf{k}_2, \mathbf{k}_3)$ to the break-up amplitude $U_0(\mathbf{p}, \mathbf{q})$ defined in Eq. (2.12), and which is related to $S(\mathbf{p}, \mathbf{q})$ as

$$S(\mathbf{p}, \mathbf{q}) = -2\pi i \delta(E'_1 + E'_{23} - E'_{lab} - E'_d) U_0(\mathbf{p}, \mathbf{q}). \quad (3.40)$$

Inserting Eq. (3.40) into Eq. (3.39) this gives

$$\begin{aligned} S(\mathbf{k}_1, \mathbf{k}_2, \mathbf{k}_3) &= -2\pi i \delta(\mathbf{k}_1 + \mathbf{k}_{23} - \mathbf{k}_{lab}) \delta(E'_1 + E'_{23} - E'_{lab} - E'_d) \\ &\quad \times \{J(\mathbf{k}_2, \mathbf{k}_3) J(\mathbf{k}_1, \mathbf{k}_{23}) J(\mathbf{k}_{lab}, \mathbf{k}_d)\}^{-\frac{1}{2}} U_0(\mathbf{p}, \mathbf{q}). \end{aligned} \quad (3.41)$$

By means of the identity

$$\begin{aligned} \delta(\mathbf{k}_1 + \mathbf{k}_{23} - \mathbf{k}_{lab}) \delta(E'_1 + E'_{23} - E'_{lab} - E'_d) \\ = \delta(\mathbf{k}_1 + \mathbf{k}_{23} - \mathbf{k}_{lab}) \delta(E_1 + E_{23} - E_{lab} - m_d) \frac{E'_1 + E'_{23} + E'_{lab} + E'_d}{E_1 + E_{23} + E_{lab} + m_d}, \end{aligned} \quad (3.42)$$

we obtain the relation between $S(\mathbf{k}_1, \mathbf{k}_2, \mathbf{k}_3)$ and $U_0(\mathbf{p}, \mathbf{q})$ as

$$\begin{aligned} S(\mathbf{k}_1, \mathbf{k}_2, \mathbf{k}_3) &= -2\pi i \delta(\mathbf{k}_1 + \mathbf{k}_{23} - \mathbf{k}_{lab}) \delta(E_1 + E_{23} - E_{lab} - m_d) \\ &\quad \times \frac{E'_1 + E'_{23} + E'_{lab} + E'_d}{E_1 + E_{23} + E_{lab} + m_d} \{J(\mathbf{k}_2, \mathbf{k}_3) J(\mathbf{k}_1, \mathbf{k}_{23}) J(\mathbf{k}_{lab}, \mathbf{k}_d)\}^{-\frac{1}{2}} U_0(\mathbf{p}, \mathbf{q}) \\ &= -2\pi i \delta(\mathbf{k}_1 + \mathbf{k}_{23} - \mathbf{k}_{lab}) \delta(E_1 + E_{23} - E_{lab} - m_d) \Gamma(\mathbf{p}, \mathbf{q}) U_0(\mathbf{p}, \mathbf{q}). \end{aligned} \quad (3.43)$$

Here the function $\Gamma(\mathbf{p}, \mathbf{q})$ is defined as

$$\begin{aligned} \Gamma(\mathbf{p}, \mathbf{q}) &\equiv \frac{E'_1 + E'_{23} + E'_{lab} + E'_d}{E_1 + E_{23} + E_{lab} + m_d} \{J(\mathbf{k}_2, \mathbf{k}_3) J(\mathbf{k}_1, \mathbf{k}_{23}) J(\mathbf{k}_{lab}, \mathbf{k}_d)\}^{-\frac{1}{2}} \\ &= \sqrt{\frac{M_{23} E'_1 E'_{23} E'_{lab} E'_d}{4 E_1 E_2 E_3 E_{lab} m_d}}. \end{aligned} \quad (3.44)$$

In the nonrelativistic limit the function $\Gamma(\mathbf{p}, \mathbf{q})$ equals 1.

IV. OBSERVABLES IN THE PROTON-NEUTRON CHARGE EXCHANGE REACTION

So far we derived the break-up amplitude $U_0(\mathbf{p}, \mathbf{q})$ in first order in its most general form. As application of a proton-deuteron break-up process we consider the (p,n) charge exchange reaction. In the experiments we are going to analyze only the scattered neutron is detected. Thus, when calculating the observables of this reaction, all possible directions of the two undetected protons must be taken into account. This is accomplished numerically by integrating over the relative direction $\hat{\mathbf{p}}$ between the two protons. In our numerical application, we consider the spin averaged differential cross section in the $d(p, n)pp$ reaction and selected spin observables. These are the neutron polarization P_0 in the $d(p, \vec{n})pp$ reaction, the analyzing power A_y in the $d(\vec{p}, n)pp$ reaction and the polarization-transfer coefficients D_{ij} in the $d(\vec{p}, \vec{n})pp$ reaction. Comprehensive descriptions and derivations of these observables can be found in e.g. Ref. [2].

The nonrelativistic cross section is given as

$$\frac{d^5 \sigma}{dE_1 d\hat{\mathbf{k}}_1} = (2\pi)^4 \frac{m^3 p k_1}{2k_{lab}} \frac{1}{6} \sum_{\substack{m_{s1} m_{s2} m_{s3} \\ m_{s1}^0 M_d}} \int d\hat{\mathbf{p}} |U_0(\mathbf{p}, \mathbf{q})|^2, \quad (4.1)$$

where \mathbf{k}_1 determines \mathbf{q} via Eq. (2.8) and p via Eqs. (2.26) and (2.8). The relativistic cross section is given by

$$d\sigma = (2\pi)^4 \frac{E_{lab}}{k_{lab}} \delta(\mathbf{k}_1 + \mathbf{k}_{23} - \mathbf{k}_{lab}) \delta(E_1 + E_{23} - E_{lab} - m_d) \times \Gamma^2(\mathbf{p}, \mathbf{q}) |U_0(\mathbf{p}, \mathbf{q})|^2 d\mathbf{k}_1 d\mathbf{k}_2 d\mathbf{k}_3, \quad (4.2)$$

where the S-matrix element from Eq. (3.43) is used, and all energies obey the relativistic energy-momentum relation. The cross section for the inclusive Nd break-up process is calculated as function of the direction $\hat{\mathbf{k}}_1$ and the kinetic energy $E_{k,1} = E_1 - m$ of the detected nucleon. Using the relation

$$d\mathbf{k}_1 = dk_1 k_1^2 d\hat{\mathbf{k}}_1 = E_1 k_1 dE_1 d\hat{\mathbf{k}}_1 = E_1 k_1 dE_{k,1} d\hat{\mathbf{k}}_1 \quad (4.3)$$

leads to

$$\begin{aligned} \frac{d\sigma}{dE_1 d\hat{\mathbf{k}}_1} &= (2\pi)^4 \frac{E_{lab} E_1 k_1}{k_{lab}} \\ &\times \int d\mathbf{k}_2 d\mathbf{k}_3 \delta(\mathbf{k}_1 + \mathbf{k}_{23} - \mathbf{k}_{lab}) \delta(E_1 + E_{23} - E_{lab} - m_d) \Gamma^2(\mathbf{p}, \mathbf{q}) |U_0(\mathbf{p}, \mathbf{q})|^2 \\ &= (2\pi)^4 \frac{E_{lab} E_1 k_1}{k_{lab}} \\ &\times \int d\mathbf{k}_{23} d\mathbf{p} J(\mathbf{k}_2, \mathbf{k}_3) \delta(\mathbf{k}_1 + \mathbf{k}_{23} - \mathbf{k}_{lab}) \delta(E_1 + E_{23} - E_{lab} - m_d) \Gamma^2(\mathbf{p}, \mathbf{q}) |U_0(\mathbf{p}, \mathbf{q})|^2 \\ &= (2\pi)^4 \frac{E_{lab} E_1 k_1}{k_{lab}} \int d\hat{\mathbf{p}} dp p^2 \frac{4E_2 E_3}{E_{23} M_{23}} \delta(E_1 + E_{23} - E_{lab} - m_d) \Gamma^2(\mathbf{p}, \mathbf{q}) |U_0(\mathbf{p}, \mathbf{q})|^2 \\ &= (2\pi)^4 \frac{E_{lab} E_1 k_1 p}{k_{lab} M_{23}} \int d\hat{\mathbf{p}} E_2 E_3 \Gamma^2(\mathbf{p}, \mathbf{q}) |U_0(\mathbf{p}, \mathbf{q})|^2. \end{aligned} \quad (4.4)$$

In addition we used Eq. (3.36) for $J(\mathbf{k}_2, \mathbf{k}_3)$ together with

$$dE_{23} = d\sqrt{M_{23}^2 + k_{23}^2} = d\sqrt{4(m^2 + p^2) + k_{23}^2} = \frac{4p}{E_{23}} dp. \quad (4.5)$$

Defining a function $\rho(p, q)$ by

$$\rho(p, q) \equiv \frac{2E_{lab} E_1 E_2 E_3}{M_{23}} \Gamma^2(\mathbf{p}, \mathbf{q}) = \frac{E'_1 E'_{23} E'_{lab} E'_d}{2m_d}, \quad (4.6)$$

allows to write the relativistic cross section similar to the nonrelativistic one, that is

$$\frac{d\sigma}{dE_1 d\hat{\mathbf{k}}_1} = (2\pi)^4 \frac{\rho(p, q) p k_1}{2k_{lab}} \frac{1}{6} \sum_{\substack{m_{s1} m_{s2} m_{s3} \\ m_{s1}^0 M_d}} \int d\hat{\mathbf{p}} |U_0(\mathbf{p}, \mathbf{q})|^2. \quad (4.7)$$

Here we restore the summation over final spins and the averaging over initial spins states. In the nonrelativistic case, the function $\rho(p, q)$ reduces to m^3 , leading to Eq. (4.1). Next we give the polarization P_0 , the analyzing power A_y and polarization-transfer coefficients $D_{ij} \equiv \frac{1}{6I_0} \text{Tr} \{ U_0(\boldsymbol{\sigma} \cdot \hat{\mathbf{j}}) U_0^\dagger(\boldsymbol{\sigma} \cdot \hat{\mathbf{i}}) \}$ as

$$P_0 = \frac{1}{6I_0} \text{Tr} \left\{ U_0 U_0^\dagger (\boldsymbol{\sigma} \cdot \hat{\mathbf{n}}) \right\} \quad (4.8)$$

$$A_y = \frac{1}{6I_0} \text{Tr} \left\{ U_0 (\boldsymbol{\sigma} \cdot \hat{\mathbf{n}}) U_0^\dagger \right\} \quad (4.9)$$

$$D_{n'n} = \frac{1}{6I_0} \text{Tr} \left\{ U_0 (\boldsymbol{\sigma} \cdot \hat{\mathbf{n}}) U_0^\dagger (\boldsymbol{\sigma} \cdot \hat{\mathbf{n}}') \right\} \quad (4.10)$$

$$D_{s's} = \frac{1}{6I_0} \text{Tr} \left\{ U_0 (\boldsymbol{\sigma} \cdot \hat{\mathbf{s}}) U_0^\dagger (\boldsymbol{\sigma} \cdot \hat{\mathbf{s}}') \right\} \quad (4.11)$$

$$D_{l's} = \frac{1}{6I_0} \text{Tr} \left\{ U_0 (\boldsymbol{\sigma} \cdot \hat{\mathbf{s}}) U_0^\dagger (\boldsymbol{\sigma} \cdot \hat{\mathbf{l}}') \right\} \quad (4.12)$$

$$D_{s'l} = \frac{1}{6I_0} \text{Tr} \left\{ U_0 (\boldsymbol{\sigma} \cdot \hat{\mathbf{l}}) U_0^\dagger (\boldsymbol{\sigma} \cdot \hat{\mathbf{s}}') \right\} \quad (4.13)$$

$$D_{l'l} = \frac{1}{6I_0} \text{Tr} \left\{ U_0 (\boldsymbol{\sigma} \cdot \hat{\mathbf{l}}) U_0^\dagger (\boldsymbol{\sigma} \cdot \hat{\mathbf{l}}') \right\}, \quad (4.14)$$

where

$$I_0 \equiv \frac{1}{6} \text{Tr} \left\{ U_0 U_0^\dagger \right\}. \quad (4.15)$$

For simplicity we suppressed the $\hat{\mathbf{p}}$ -integration in Eqs. (4.8)-(4.15). The unit vectors $\hat{\mathbf{n}}, \hat{\mathbf{l}}, \hat{\mathbf{s}}, \hat{\mathbf{n}}', \hat{\mathbf{l}}'$ and $\hat{\mathbf{s}}'$ are defined as

$$\hat{\mathbf{n}} = \hat{\mathbf{n}}' \equiv \frac{\mathbf{k}_{lab} \times \mathbf{k}_1}{|\mathbf{k}_{lab} \times \mathbf{k}_1|}, \quad \hat{\mathbf{l}} \equiv \hat{\mathbf{k}}_{lab}, \quad \hat{\mathbf{s}} \equiv \hat{\mathbf{n}} \times \hat{\mathbf{l}}, \quad \hat{\mathbf{l}}' \equiv \hat{\mathbf{k}}_1, \quad \hat{\mathbf{s}}' \equiv \hat{\mathbf{n}}' \times \hat{\mathbf{l}}'. \quad (4.16)$$

For the explicit calculation of the Nd break-up amplitude $U_0(\mathbf{p}, \mathbf{q})$, Eq. (2.47), we need the NN T-matrix elements. They are obtained by solving the Lippmann- Schwinger (LS) equations for a given NN potential in 3D as described in Ref. [7] at fixed momenta, angles, and energies. The matrix elements $T_{\Lambda\Lambda'}^{\pi St}(p, \pi, \cos\theta'; E_p)$ are then obtained by interpolating in $\pi, \cos\theta',$ and E_p . This is more economic than solving the LS equation every time for the corresponding energies and initial momenta. Similarly the partial wave deuteron wave function components are calculated once and interpolated to the momenta π' . For all the interpolations we use the modified cubic Hermite splines of Ref. [16]. Typical grid sizes for our calculations are 40 points for E_p (and p), 80 points for $\cos\theta'$, and 50 points for π . This grid is then used for all our break-up calculations from 5 to 500 MeV.

V. RESULTS AND DISCUSSION

Our numerical calculations are based two different NN potentials, the Bonn-B [17] and AV18 [18] potentials. In the discussion of our results we consider three different aspects. First, since we present a new way of calculating the break-up process, namely without partial wave decomposition, we need to compare our results to those obtained in traditional partial wave based calculations. After having established the feasibility and correctness of our calculations, we will address two physical questions, namely the importance of rescattering contributions in the (p,n) charge exchange reaction at a moderately high energy and the effect of different descriptions of the kinematics, i.e. we compare the relativistic treatment introduced in Section III to the nonrelativistic description.

A. Comparison with Partial-Wave Calculations

In this section we compare our 3D calculations with traditional PW calculations at different energies. The aim here is twofold. First, we want to convince ourselves that our newly developed 3D formulations agrees with well established PW calculations [19]. Secondly, we want to find out from which energy regime on our 3D method surpasses the state-of-the-art PW calculations. As already mentioned in the introduction, in PW calculations the number of partial waves necessary for a converged result proliferated as the energies increases, leading to limitations with respect to computational feasibility and accuracy. Our new 3D scheme does not suffer from these limitations, the computational effort is in principle independent of the projectile energy considered.

Our first comparison is carried out at a proton incident energy of $E_{lab} = 100$ MeV and a neutron laboratory scattering angle $\theta_{lab} = 13^\circ$. The calculations, which are based on the Bonn-B potential are given in Fig. 1, which shows the differential cross section, the analyzing power A_y and the polarization-transfer coefficient D_{sl} . The solid lines represent our 3D calculations, the dashed lines the corresponding PW calculations [19]. Here we use the notation j for the highest 2N total angular momentum taken into account in the PW calculation, and J for the highest 3N total angular momentum. The figure shows that both lines are almost indistinguishable, thus validating our new scheme. At this point we also would like to mention, that the channels used in the PW calculation, namely $j = 7$ and $J = 31/2$ constitute todays limits for a PW calculation. In addition, we carried out comparisons at lower energies, e.g. at 16 MeV, where a PW calculation with $j = 5$ and $J = 31/2$ is in perfect agreement with our 3D calculations.

Next, we turn to a slightly higher projectile energy, $E_{lab} = 197$ MeV, and carry out the same comparison. The results for the differential cross section, the analyzing power A_y and the polarization-transfer coefficient D_{sl} are shown in Fig. 2, where the solid line represents our 3D calculation. The PW calculations are shown with increasing number of partial waves from $j = 5, J = 25/2$ to $j = 7, J = 31/2$. The peak of the differential cross section reveals that each additional angular momentum of the PW calculation results in an additive contribution, but even the highest possible number deviates about 9% from our 3D result. This is the most extreme case, for the analyzing power A_y and the polarization-transfer coefficient D_{sl} the PW calculation with $j = 7$ and $J = 31/2$ agrees reasonable well with our 3D result. It is interesting to note that for D_{sl} the 2N total momentum j is much more important to reach convergence than the total 3N momentum J .

At this point it is appropriate to make some general remarks. In this work we restrict our 3D approach to the leading term in the Faddeev multiple scattering series. Thus we have no insight whether the fully summed series would lead to a better agreement of 3D and PW approach. We also restrict ourselves to semi-exclusive processes, and can not draw any conclusions on 3D and PW calculations with respect to elastic scattering observables or full break-up observables. But nevertheless, the comparison in Fig. 2 indicates that around 200 MeV the convergence of the PW approach has to be carefully checked.

B. Contributions from the Rescattering Terms

One of the arguments to study the semi-exclusive Nd break-up process in first order in the NN T-matrix is that at higher energies the rescattering term generated by the solution of the full Faddeev equations become less important. For a comprehensive study of the importance of those rescattering terms it would be necessary to compare first order calculations with full Faddeev calculations over a wide range of projectile energies and for many different experimental situations. Unfortunately we can not do this at the present stage, since three-dimensional full Faddeev calculations do not yet exist, and traditional, partial wave based Faddeev calculations are limited in their energy range. Thus we take as compromise a medium energy of about 200 MeV, and compare the (p,n) charge exchange observables calculated in our first order 3D approach with the ones obtained from a full, partial wave based Faddeev calculation. We choose the proton energy $E_{lab}=197$ MeV, since there exist recent measurements [8].

Our calculations are based on two different NN potential models, namely Bonn-B [17] and AV18 [18]. Both potentials are defined below 350 MeV nucleon laboratory energy, which corresponds to a NN c.m. energy of 175 MeV. In the Nd break-up process in first order the NN c.m. energy available to the two-nucleon subsystem is fixed in terms of the laboratory momentum of the final nucleon and the projectile energy. For a projectile energy of about 200 MeV in the pd scattering process, the maximum NN c.m. energy in the two-body subsystem is about 133 MeV. Thus, our calculations employ the NN models in an energy regime, where they are perfectly well defined. Of course, the two potential models exhibit differences in the description of the NN phase shifts. The model AV18 is one of the socalled high-precision potentials, describing the NN data base with a $\chi^2/datum \approx 1$, whereas Bonn-B has a slightly higher $\chi^2/datum$ value. Thus, there are on-shell differences between those two models, which should lead to differences in the Nd break-up observables.

In Figs. 3 and 4 we compare the 3D calculations with PW based full Faddeev calculations [19] at 197 MeV proton energy. We show the spin averaged differential cross section, the analyzing power and polarization-transfer coefficients at two angles, $\theta_{lab} = 24^\circ$ and $\theta_{lab} = 37^\circ$ together with experimental results from Ref. [8]. The PW full Faddeev calculations use $j = 5, J = 31/2$ for the AV18 NN potential, and $j = 4, J = 31/2$ for the Bonn-B NN potential. Since the solution of the PW full Faddeev equations is more involved we restrict ourselves to a lower number of partial waves. However, the number of partial waves is sufficient to study the importance of rescattering terms in the multiple scattering series at this energy. The first obvious difference between the two calculations is the appearance of the final state peak in the differential cross section, which of course is solely due to rescattering. Furthermore, we see that rescattering contributions have the general tendency to push the peak of the differential cross section down, though the size of the effect depends on the angle and the potential. However, the rescattering terms do not affect the position of the peak. We see that the peak is shifted further away from the data the larger the neutron scattering angle becomes. For both angles, the analyzing power A_y shows the largest effect of rescattering for small neutron energies, which can be expected, since interactions between outgoing particles should be larger, when their relative energy is smaller. In both cases, A_y can only be satisfactorily described when rescattering terms are taken into account. For the polarization-transfer coefficient D_{ll} at $\theta_{lab} = 24^\circ$ the situation is similar, rescattering effects

are largest for small neutron energies. For D_{ss} at $\theta_{lab} = 37^\circ$ none of the calculations is able to capture the general shape of the data, rescattering effects are visible, but they do not affect the general shape of the curve as this is the case in the other observables shown in Figs. 3 and 4. From these consideration we have to conclude, that at a projectile energy $E_{lab} \simeq 200$ MeV rescattering terms still give considerable contributions to the full pd break-up amplitude and hence cannot be neglected. Due to the lack of calculations based on the full Faddeev equations at higher energies, we can not carry out corresponding studies at higher energies.

C. Relativistic Effects

In this section we study the effects of relativistic kinematics in the break-up amplitude and follow the formulation derived in Section III. We also want to take full advantage of our 3D formulation and carry out calculations at proton incident energies higher than 200 MeV, a regime where partial wave based Faddeev calculations become less competitive. Of course we also realize that the NN potentials from which our NN T-matrix is obtained are strictly speaking out of their range of validity, i.e. they do not include important Delta degrees of freedom. A NN laboratory energy of 350 MeV roughly corresponds to a proton incident laboratory energy of 260 MeV in the pd scattering process. A comparison of the NN scattering observables with the calculated ones shows that even at NN laboratory energies higher than 350 MeV the agreement with data deteriorates relatively slowly. Nevertheless, this can lead to deficiencies in describing the Nd break-up process at $E_{lab} > 260$ MeV.

At first we investigate the effect of relativistic kinematics on the break-up observables at a low energy, $E_{lab} = 100$ MeV, where it is expected to be small. In Fig. 5 we show the differential cross section and A_y at $E_{lab} = 100$ MeV and a neutron laboratory scattering angle $\theta_{lab} = 24^\circ$. In the cross section effects are only visible in the quasi-free-scattering (QFS) peak, but in general one can say that around 100 MeV relativistic effects are small, and certainly not the dominant correction to worry about.

Going to a higher energy, $E_{lab} = 197$ MeV, the relativistic effects increase considerably. In Figs. 6 and 7 we show the cross section and A_y and two polarization-transfer coefficients at neutron laboratory scattering angles $\theta_{lab} = 24^\circ$ and $\theta_{lab} = 37^\circ$. Here the QFS peak is visibly enhanced by the use of relativistic kinematics. More importantly, its location is shifted towards smaller neutron energies, and is now in better agreement with the experimentally determined peak location. As far as the spin observables are concerned, the relativistic corrections show the largest effect for the higher neutron energies.

A proton energy of $E_{lab} = 346$ MeV is the next higher energy at which the (p,n) charge exchange reaction is measured [9]. In Fig. 8 we display 3D calculations with nonrelativistic and relativistic kinematics for a neutron scattering angle $\theta_{lab} = 22^\circ$. Again we observe an increase in the QFS peak and a shift to lower neutron energies. Here we would like to point out that there is an uncertainty in the data as far as the location of the QFS peak is concerned. In the experiment there is an uncertainty of the energy, at which the pd break-up process exactly occurs. For example, due to the thickness of the target the proton may have lost some of its energy before it hits and breaks the deuteron apart [19]. In this case, the break-up process occurs at an energy slightly different from the calculated one. The effect of relativistic kinematics on the spin observables is clearly more pronounced compared

to $E_{lab} = 197$ MeV. We also calculate the break-up process at $E_{lab} = 495$ MeV, though here the uncertainty with respect to our input NN interactions is largest. In Fig. 9 we show the differential cross section, A_y and D_{ll} at $E_{lab} = 495$ MeV for a neutron laboratory scattering angle $\theta_{lab} = 18^\circ$ together with the measurements from Ref. [21]. Here we clearly see that the corrections due to relativistic kinematics push the QFS peak towards lower neutron energies, and the location of our calculated peak agrees with the measured one. The effects on the spin observables are now also quite sizable.

With this study we can qualitatively indicate that relativistic effects become important when going to higher energies. However, we can not make any definite statements, since we only consider relativistic kinematics. We have not considered effects resulting from boosting the NN T-matrix [10] and Wigner rotations of the spin [11]. Those effects in principle could counterbalance the kinematic effects. It also remains to be seen, how important rescattering effects will be at those higher energies. Our calculations based on the first order term and relativistic kinematics overestimate the differential cross section. That could imply, that rescattering still plays an important role at those energies.

VI. SUMMARY AND CONCLUSIONS

We formulate and calculate the Nd break-up process based on the Faddeev scheme in first order in the multiple scattering expansion in a three-dimensional fashion which does not rely on any partial wave decomposition. The leading term for the Nd break-up amplitude is derived in a representation, which uses directly the momentum vectors. This representation can be connected to the momentum-helicity basis, in which we solve for the NN T-matrix in a 3D fashion. Special care has to be taken when rotating the NN T-matrix elements, which occur with arbitrarily oriented initial momenta in the Nd break-up amplitude, such that the NN initial relative momenta point into a fixed z-direction. This is needed since two nucleon LS equation for the NN T-matrix is solved in a basis where the arbitrary z-axis points into the direction of the initial momenta. This leads to an intricate additional phase factor.

As specific application of our new formulation we calculate the (p,n) charge exchange reaction in the proton-deuteron break-up process. Here only the outgoing neutron is detected after the break-up. Our calculations concentrate on spin averaged differential cross sections, neutron polarizations, proton analyzing powers, and polarization-transfer coefficients at different energies.

First we carry out calculations of observables for the leading order term in the NN T-matrix at energies which are accessible to traditional, partial wave based Faddeev calculations. The aim here is twofold. First, we need to establish the numerical accuracy and feasibility of our new formulation. We establish both by comparing observables calculated in both schemes at a proton incident energy $E_{lab} = 100$ MeV, where we find excellent agreement between both calculations. At $E_{lab} = 200$ MeV we find some slight deviations between the two schemes, especially in the quasi-free peak of the differential cross section. This can be identified as the onset of a lack of convergence using the typical and feasible number of partial waves in the traditional partial wave based calculation in that particular observable. From that we conclude that starting at about 200 MeV, the convergence of partial wave based calculations has to be checked carefully.

Second, we want to investigate the importance of rescattering terms at a moderately high energy. Of course, we need full Faddeev calculations here. Since those do not yet exist in a 3D formulation using realistic NN potentials, we have to resort to partial wave based full Faddeev calculations. This of course limits the energy regime we can study. Thus, we compare our calculations at $E_{lab} = 197$ MeV to the PW full Faddeev calculations. We find that at this energy rescattering effects are still important, and are mostly visible in the cross section and the analyzing power. In addition, we find that the PW full Faddeev calculations provide a reasonable description of the (p,n) charge exchange reaction at 200 MeV. However, we also can detect one obvious deficiency in both schemes, at larger neutron laboratory scattering angles the QFS peak is located at slightly too high neutron energies compared to the data.

This leads to the next topic we investigate, namely the effect of relativistic kinematics in the Nd break-up reaction. Here we have to employ not only relativistic energy-momentum relations, but also need to reevaluate the Jacobi momenta by carrying out corresponding Lorentz transformations to the two- and three-particle c.m. subsystems, and employ a relativistic description of the cross section. We compare our 3D calculation based on non-relativistic kinematics with the corresponding one based on relativistic kinematics. Though there are no sizable effects at 100 MeV proton incident energy, we find, that at 200 MeV visible effect occur, mainly the differential cross section. Its magnitude increases, but most importantly, the QFS peak is shifted to the experimentally determined one using relativistic kinematics. Since our calculations are as easily carried out at 300 or 500 MeV as at 200 MeV, we perform calculations at $E_{lab}=346$ MeV and 497 MeV, where experimental data are available. We find that at those higher energies the effects due to the relativistic kinematics are considerably larger than at 200 MeV. They are now visible not only in the cross section but also in the spin observables. Even at $E_{lab}=500$ MeV this specific feature prevails, namely that the QFS peak is shifted to lower neutron energies and coincides now with the experimentally determined one. However, its magnitude is larger. With these finding we can qualitatively indicate that relativistic effects become increasingly important when considering the Nd break-up reaction at higher energies. However, we have to exercise some caution in the interpretation of our findings, since we have not considered dynamical relativistic effects, such as boosting of the NN T-matrix. It also remains to be seen how important rescattering effects will be in the higher energy regime.

Summarizing, for the first order term in the multiple scattering series in the Faddeev scheme the 3D approach has proven to be a viable alternative to the established partial wave based calculations. When entering the intermediate energy regime it may be the approach having the most promise of being successful in the near future, due to the intrinsic limitations with respect to computational feasibility and accuracy faced by partial wave calculations at higher energies. It is also clear that the 3D approach, though having a well defined roadmap ahead, is still facing extensive development needs. The full Faddeev equations will have to be solved, with the inclusion of three-nucleon forces, which may play a more dominant role at higher energies. Furthermore, though we consider the effects of relativistic kinematics, we have not taken into account the corresponding dynamical effects. And last, but not least, the underlying input of any 3N calculation, namely the two-nucleon force, is by far less developed at higher energies than it is for energies below the pion production threshold.

ACKNOWLEDGMENTS

We would like to thank Henryk Witała and Jacek Golak for very useful discussions and providing the PW results. This work was performed in part under the auspices of the Deutsche Akademische Austauschdienst under contract No. A/96/32258, and the U. S. Department of Energy under contract No. DE-FG02-93ER40756 with Ohio University. We thank the Computer Center of the RWTH Aachen (Grant P039) for the use of their facilities.

APPENDIX A: TWO SUCCESSIVE ROTATIONS

In this appendix we evaluate the rotation of the state $|\mathbf{p}; \hat{p}S\Lambda\rangle$ as

$$R^\dagger(\hat{\mathbf{p}}') |\mathbf{p}; \hat{p}S\Lambda\rangle = R(0, -\theta', -\phi') R(\phi\theta0) |p\hat{\mathbf{z}}; \hat{\mathbf{z}}S\Lambda\rangle. \quad (\text{A1})$$

First, we give a few basic definitions and relations required to follow the calculation. More details about rotation can be found in e.g. Ref. [13].

A general rotation operator $R(\hat{\mathbf{p}})$ is defined as

$$R(\hat{\mathbf{p}}) = R(\phi\theta0) = e^{-iJ_z\phi} e^{-iJ_y\theta}, \quad (\text{A2})$$

where J_z, J_y are the z- and y-components of the angular momentum operator \mathbf{J} and (θ, ϕ) the rotation angles that determine the direction of \mathbf{p} . This operator rotates the angular momentum state $|\hat{\mathbf{z}}jm\rangle$ into the state $|\hat{\mathbf{p}}jm\rangle$,

$$|\hat{\mathbf{p}}jm\rangle = R(\hat{\mathbf{p}})|\hat{\mathbf{z}}jm\rangle = \sum_{m'} D_{m'm}^j(\hat{\mathbf{p}}) |\hat{\mathbf{z}}jm'\rangle, \quad (\text{A3})$$

where $D_{m'm}^j(\hat{\mathbf{p}})$ are the Wigner D-function defined as

$$D_{m'm}^j(\hat{\mathbf{p}}) = D_{m'm}^j(\phi\theta0) \equiv \langle \hat{\mathbf{z}}jm' | R(\hat{\mathbf{p}}) | \hat{\mathbf{z}}jm \rangle. \quad (\text{A4})$$

A rotation $R(\alpha\beta\gamma)$ corresponds to a change of the Cartesian coordinates \mathbf{r} describing the state. The new Cartesian coordinates \mathbf{r}' are related to the old ones \mathbf{r} as

$$\mathbf{r}' = M(\alpha\beta\gamma)\mathbf{r}, \quad (\text{A5})$$

where the rotation matrix $M(\alpha\beta\gamma)$ is given as

$$M(\alpha\beta\gamma) = \begin{pmatrix} \cos\alpha\cos\beta\cos\gamma - \sin\alpha\sin\gamma & \sin\alpha\cos\beta\cos\gamma + \cos\alpha\sin\gamma & -\sin\beta\cos\gamma \\ -\cos\alpha\cos\beta\sin\gamma - \sin\alpha\cos\gamma & -\sin\alpha\cos\beta\sin\gamma + \cos\alpha\cos\gamma & \sin\beta\sin\gamma \\ \cos\alpha\sin\beta & \sin\alpha\sin\beta & \cos\beta \end{pmatrix}. \quad (\text{A6})$$

1. Two Successive Rotations in Momentum Space

We denote the rotation operator in momentum space as $R_L(\hat{\mathbf{p}})$, which is given in term of the orbital angular momentum operator \mathbf{L} as

$$R_L(\hat{\mathbf{p}}) = R_L(\phi\theta0) = e^{-iL_z\phi} e^{-iL_y\theta}. \quad (\text{A7})$$

A momentum state $|\mathbf{p}\rangle$ with $\hat{\mathbf{p}}$ pointing in the direction (θ, ϕ) can be expanded in partial waves as

$$|\mathbf{p}\rangle = \sum_{lm} |plm\rangle Y_{lm}^*(\theta, \phi), \quad (\text{A8})$$

where $|plm\rangle$ is defined to be quantized along the z-axis. The state $|\mathbf{p}\rangle$ can be obtained by rotating a state $|p\hat{\mathbf{z}}\rangle$ as follows,

$$\begin{aligned}
R_L(\hat{\mathbf{p}})|p\hat{\mathbf{z}}\rangle &= R_L(\phi\theta0)\sum_{lm}|plm\rangle Y_{lm}^*(0,0) \\
&= R_L(\phi\theta0)\sum_l|pl0\rangle\sqrt{\frac{2l+1}{4\pi}} \\
&= \sum_l\sum_{l'm}|pl'm\rangle\langle\hat{\mathbf{z}}l'm|R_L(\phi\theta0)|\hat{\mathbf{z}}l0\rangle\sqrt{\frac{2l+1}{4\pi}} \\
&= \sum_{lm}|plm\rangle D_{m0}^l(\phi\theta0)\sqrt{\frac{2l+1}{4\pi}} \\
&= \sum_{lm}|plm\rangle Y_{lm}^*(\theta,\phi) \\
&= |\mathbf{p}\rangle.
\end{aligned} \tag{A9}$$

Here we used the relation between the spherical harmonics and the Wigner D-functions,

$$Y_{lm}^*(\theta,\phi) = \sqrt{\frac{2l+1}{4\pi}}D_{m0}^l(\phi\theta0). \tag{A10}$$

Now we rotate the state $|\mathbf{p}\rangle$ with an inverse rotation operator $R_L^{-1}(\hat{\mathbf{p}}') = R_L^\dagger(\hat{\mathbf{p}}') = R_L(0, -\theta', -\phi')$. It follows that

$$\begin{aligned}
R_L^\dagger(\hat{\mathbf{p}}')|\mathbf{p}\rangle &= R_L^\dagger(\hat{\mathbf{p}}')\sum_{lm}|plm\rangle Y_{lm}^*(\theta,\phi) \\
&= \sum_{lm}\sum_{l'm'}|pl'm'\rangle\langle\hat{\mathbf{z}}l'm'|R_L^\dagger(\hat{\mathbf{p}}')|\hat{\mathbf{z}}lm\rangle Y_{lm}^*(\theta,\phi) \\
&= \sum_{lm}\sum_{l'm'}|pl'm'\rangle\langle\hat{\mathbf{z}}l'm'|R_L^\dagger(\hat{\mathbf{p}}')|\hat{\mathbf{z}}lm\rangle\langle\hat{\mathbf{z}}lm|\hat{\mathbf{p}}\rangle \\
&= \sum_{l'm'}|pl'm'\rangle\langle\hat{\mathbf{z}}l'm'|R_L^\dagger(\hat{\mathbf{p}}')|\hat{\mathbf{p}}\rangle \\
&\equiv \sum_{l'm'}|pl'm'\rangle\langle\hat{\mathbf{z}}l'm'|\hat{\mathbf{p}}''\rangle \\
&= \sum_{l'm'}|pl'm'\rangle Y_{l'm'}^*(\theta'',\phi'') \\
&= R_L(\hat{\mathbf{p}}'')|p\hat{\mathbf{z}}\rangle,
\end{aligned} \tag{A11}$$

where we have defined a direction $\hat{\mathbf{p}}''$ to be determined by $\hat{\mathbf{p}}$ and $\hat{\mathbf{p}}'$ according to

$$|\hat{\mathbf{p}}''\rangle = R_L^\dagger(\hat{\mathbf{p}}')|\hat{\mathbf{p}}\rangle. \tag{A12}$$

Inserting Eq. (A9) into Eq. (A11) this leads to

$$R_L^\dagger(\hat{\mathbf{p}}')R_L(\hat{\mathbf{p}})|p\hat{\mathbf{z}}\rangle = R_L(\hat{\mathbf{p}}'')|p\hat{\mathbf{z}}\rangle. \tag{A13}$$

Hence, the two successive rotations $R_L^\dagger(\hat{\mathbf{p}}')R_L(\hat{\mathbf{p}})$ applied to the state $|p\hat{\mathbf{z}}\rangle$ can be replaced by the single rotation $R_L(\hat{\mathbf{p}}'')$. Consequently any number of successive rotations in momentum

space can always be replaced by one rotation with the corresponding rotation angles. The angles (θ'', ϕ'') of \mathbf{p}'' are determined by the angles (θ, ϕ) of \mathbf{p} and (θ', ϕ') of \mathbf{p}' by

$$\cos \theta'' = \cos \theta \cos \theta' + \sin \theta \sin \theta' \cos(\phi - \phi') \quad (\text{A14})$$

$$\sin \theta'' e^{i\phi''} = -\cos \theta \sin \theta' + \sin \theta \cos \theta' \cos(\phi - \phi') + i \sin \theta \sin(\phi - \phi'), \quad (\text{A15})$$

and are obtained from the rotation matrices of the Cartesian coordinates, which correspond to the rotations in Eq. (A13). Such a rotation matrix $M(\alpha\beta\gamma)$ corresponding to $R(\alpha\beta\gamma)$ is given in Eq. (A6).

2. Two Successive Rotations in Spin Space

We denote the rotation operator in spin space as $R_S(\hat{\mathbf{p}})$, which is given in term of the total spin operator \mathbf{S} as

$$R_S(\hat{\mathbf{p}}) = R_S(\phi\theta0) = e^{-iS_z\phi} e^{-iS_y\theta}. \quad (\text{A16})$$

The rotation identity given in Eq. (A13) may not apply in spin space. Therefore, we evaluate two successive rotations in spin space, independent of the evaluation in momentum space. We compare the rotated spin state or the helicity state $|\hat{\mathbf{p}}''S\Lambda\rangle_I$ with $|\hat{\mathbf{p}}''S\Lambda\rangle_{II}$ given by

$$|\hat{\mathbf{p}}''S\Lambda\rangle_I = R_S(\hat{\mathbf{p}}'')|\hat{\mathbf{z}}S\Lambda\rangle \quad (\text{A17})$$

$$|\hat{\mathbf{p}}''S\Lambda\rangle_{II} = R_S^\dagger(\hat{\mathbf{p}}')R_S(\hat{\mathbf{p}})|\hat{\mathbf{z}}S\Lambda\rangle. \quad (\text{A18})$$

It should be pointed out that here the relation between (θ'', ϕ'') , (θ', ϕ') and (θ, ϕ) given in Eqs. (A14) and (A15) is still valid, since transformations of the Cartesian coordinates are the same in both momentum space and spin space.

Both states $|\hat{\mathbf{p}}''S\Lambda\rangle_I$ and $|\hat{\mathbf{p}}''S\Lambda\rangle_{II}$ are eigenstates of the helicity operator $\mathbf{S} \cdot \hat{\mathbf{p}}''$ with eigenvalue Λ , as can be shown as follows:

$$\begin{aligned} \mathbf{S} \cdot \hat{\mathbf{p}}''|\hat{\mathbf{p}}''S\Lambda\rangle_I &= R_S(\hat{\mathbf{p}}'')\mathbf{S} \cdot \hat{\mathbf{z}}R_S^\dagger(\hat{\mathbf{p}}'')R_S(\hat{\mathbf{p}}'')|\hat{\mathbf{z}}S\Lambda\rangle \\ &= R_S(\hat{\mathbf{p}}'')\mathbf{S} \cdot \hat{\mathbf{z}}|\hat{\mathbf{z}}S\Lambda\rangle \\ &= \Lambda R_S(\hat{\mathbf{p}}'')|\hat{\mathbf{z}}S\Lambda\rangle \\ &= \Lambda|\hat{\mathbf{p}}''S\Lambda\rangle_I \end{aligned} \quad (\text{A19})$$

$$\begin{aligned} \mathbf{S} \cdot \hat{\mathbf{p}}''|\hat{\mathbf{p}}''S\Lambda\rangle_{II} &= R_S^\dagger(\hat{\mathbf{p}}')R_S(\hat{\mathbf{p}})\mathbf{S} \cdot \hat{\mathbf{z}}R_S^\dagger(\hat{\mathbf{p}})R_S(\hat{\mathbf{p}}')R_S^\dagger(\hat{\mathbf{p}}')R_S(\hat{\mathbf{p}})|\hat{\mathbf{z}}S\Lambda\rangle \\ &= R_S^\dagger(\hat{\mathbf{p}}')R_S(\hat{\mathbf{p}})\mathbf{S} \cdot \hat{\mathbf{z}}|\hat{\mathbf{z}}S\Lambda\rangle \\ &= \Lambda R_S^\dagger(\hat{\mathbf{p}}')R_S(\hat{\mathbf{p}})|\hat{\mathbf{z}}S\Lambda\rangle \\ &= \Lambda|\hat{\mathbf{p}}''S\Lambda\rangle_{II}. \end{aligned} \quad (\text{A20})$$

Moreover, because of the unitarity transformations in Eqs. (A17) and (A18) the two states have the same norm and can at most differ by a phase factor.

The helicity states $|\hat{\mathbf{p}}''S\Lambda\rangle_I$ and $|\hat{\mathbf{p}}''S\Lambda\rangle_{II}$ are expanded in the spin states $|\hat{\mathbf{z}}S\Lambda\rangle$ as

$$|\hat{\mathbf{p}}''S\Lambda\rangle_I = R_S(\hat{\mathbf{p}}'')|\hat{\mathbf{z}}S\Lambda\rangle = \sum_{\Lambda'}|\hat{\mathbf{z}}S\Lambda'\rangle D_{\Lambda'\Lambda}^S(\phi''\theta''0) \quad (A21)$$

$$\begin{aligned} |\hat{\mathbf{p}}''S\Lambda\rangle_{II} &= R_S^\dagger(\hat{\mathbf{p}}')R_S(\hat{\mathbf{p}}')|\hat{\mathbf{z}}S\Lambda\rangle \\ &= \sum_{\Lambda'N}|\hat{\mathbf{z}}S\Lambda'\rangle\langle\hat{\mathbf{z}}S\Lambda'|R_S^\dagger(\phi'\theta'0)|\hat{\mathbf{z}}SN\rangle\langle\hat{\mathbf{z}}SN|R_S(\phi\theta0)|\hat{\mathbf{z}}S\Lambda\rangle \\ &= \sum_{\Lambda'}|\hat{\mathbf{z}}S\Lambda'\rangle\sum_N D_{N\Lambda'}^{S*}(\phi'\theta'0)D_{N\Lambda}^S(\phi\theta0) \\ &\equiv \sum_{\Lambda'}|\hat{\mathbf{z}}S\Lambda'\rangle X_{\Lambda'\Lambda}^S(\phi''\theta''0), \end{aligned} \quad (A22)$$

where

$$X_{\Lambda'\Lambda}^S(\phi''\theta''0) \equiv \sum_N D_{N\Lambda'}^{S*}(\phi'\theta'0)D_{N\Lambda}^S(\phi\theta0). \quad (A23)$$

Therefore, instead of comparing $|\hat{\mathbf{p}}''S\Lambda\rangle_I$ with $|\hat{\mathbf{p}}''S\Lambda\rangle_{II}$ we compare $D_{\Lambda'\Lambda}^S(\phi''\theta''0)$ with $X_{\Lambda'\Lambda}^S(\phi''\theta''0)$, since these are known functions. We have two spin cases $S = 0$ and $S = 1$. For $S = 0$ the spin state is rotationally invariant and thus we can immediately get

$$X_{00}^0(\phi''\theta''0) = D_{00}^0(\phi''\theta''0) = 1 \quad (A24)$$

and correspondingly

$$|\hat{\mathbf{p}}''00\rangle_I = |\hat{\mathbf{p}}''00\rangle_{II} = |\hat{\mathbf{z}}00\rangle. \quad (A25)$$

For $S = 1$ we make use of a symmetry relation for the Wigner D-functions given as

$$D_{m'm}^{j*}(\alpha\beta\gamma) = (-)^{m'-m}D_{-m',-m}^j(\alpha\beta\gamma), \quad (A26)$$

allowing to leave out the case with initial helicity $\Lambda = -1$ and consider only six cases with $\Lambda' = 1, 0, -1$ and $\Lambda = 1, 0$.

The Wigner D-function $D_{\Lambda'\Lambda}^1(\phi\theta0)$ is given as

$$D^1(\phi\theta0) = \begin{pmatrix} e^{-i\phi}\frac{1+\cos\theta}{2} & -e^{-i\phi}\frac{\sin\theta}{\sqrt{2}} & e^{-i\phi}\frac{1-\cos\theta}{2} \\ \frac{\sin\theta}{\sqrt{2}} & \cos\theta & -\frac{\sin\theta}{\sqrt{2}} \\ e^{i\phi}\frac{1-\cos\theta}{2} & e^{i\phi}\frac{\sin\theta}{\sqrt{2}} & e^{i\phi}\frac{1+\cos\theta}{2} \end{pmatrix}. \quad (A27)$$

For $\Lambda = 0$ it follows that

$$X_{10}^1(\phi''\theta''0) = -e^{-i\phi''}\frac{\sin\theta''}{\sqrt{2}} = D_{10}^1(\phi''\theta''0) \quad (A28)$$

$$X_{00}^1(\phi''\theta''0) = \cos\theta'' = D_{00}^1(\phi''\theta''0) \quad (A29)$$

$$X_{-10}^1(\phi''\theta''0) = e^{i\phi''}\frac{\sin\theta''}{\sqrt{2}} = D_{-10}^1(\phi''\theta''0), \quad (A30)$$

and thus,

$$X_{\Lambda'0}^1(\phi''\theta''0) = D_{\Lambda'0}^1(\phi''\theta''0) \quad (A31)$$

and correspondingly

$$|\hat{\mathbf{p}}''10\rangle_{\text{I}} = |\hat{\mathbf{p}}''10\rangle_{\text{II}}. \quad (\text{A32})$$

For $\Lambda = 1$ we obtain

$$\begin{aligned} X_{11}^1(\phi''\theta''0) &= \frac{1}{2} \{ (1 + \cos \theta \cos \theta') \cos(\phi - \phi') + \sin \theta \sin \theta' \} \\ &\quad - \frac{i}{2} (\cos \theta + \cos \theta') \sin(\phi - \phi') \end{aligned} \quad (\text{A33})$$

$$X_{01}^1(\phi''\theta''0) = \frac{1}{\sqrt{2}} \{ -\cos \theta \sin \theta' \cos(\phi - \phi') + \sin \theta \cos \theta' + i \sin \theta' \sin(\phi - \phi') \} \quad (\text{A34})$$

$$\begin{aligned} X_{-11}^1(\phi''\theta''0) &= \frac{1}{2} \{ (1 - \cos \theta \cos \theta') \cos(\phi - \phi') - \sin \theta \sin \theta' \} \\ &\quad - \frac{i}{2} (\cos \theta - \cos \theta') \sin(\phi - \phi'). \end{aligned} \quad (\text{A35})$$

Hence, for $\Lambda = 1$ apparently $X_{\Lambda'1}^1(\phi''\theta''0)$ differs from $D_{\Lambda'1}^1(\phi''\theta''0)$, and correspondingly $|\hat{\mathbf{p}}''11\rangle_{\text{II}}$ from $|\hat{\mathbf{p}}''11\rangle_{\text{I}}$, by a phase factor. Now the difference between Eqs. (A28)-(A30) and Eqs. (A33)-(A35) is connected to the value of Λ . Therefore, the phase factor must depend on Λ and is independent of Λ' . The latter can be understood as we see that there is no Λ' -dependence in Eqs. (A17) and (A18). In addition the phase factor also depends on the set of angles $(\phi, \theta, \phi', \theta')$. Thus we write

$$X_{\Lambda'\Lambda}^1(\phi''\theta''0) = e^{i\Omega\Lambda} D_{\Lambda'\Lambda}^1(\phi''\theta''0), \quad (\text{A36})$$

where Ω depends on the set of angles $(\phi, \theta, \phi', \theta')$. Noting that $D_{01}^1(\phi''\theta''0)$ is real the phase Ω can be given through its tangential as

$$\tan \Omega = \frac{\text{Im}\{X_{01}^1(\phi''\theta''0)\}}{\text{Re}\{X_{01}^1(\phi''\theta''0)\}} = \frac{\sin \theta' \sin(\phi - \phi')}{-\cos \theta \sin \theta' \cos(\phi - \phi') + \sin \theta \cos \theta'}. \quad (\text{A37})$$

The Ω calculated in Eq. (A37) is also valid for other combinations of Λ' and Λ , since Ω is independent of Λ' and Λ . After all these evaluations we summarize that

$$R_S^\dagger(\hat{\mathbf{p}}') R_S(\hat{\mathbf{p}}') |\hat{\mathbf{z}}S\Lambda\rangle = e^{i\Omega\Lambda} R_S(\hat{\mathbf{p}}'') |\hat{\mathbf{z}}S\Lambda\rangle \quad (\text{A38})$$

$$e^{i\Omega\Lambda} = \frac{\sum_{N=-S}^S D_{N\Lambda'}^{S*}(\phi'\theta'0) D_{N\Lambda}^S(\phi\theta0)}{D_{\Lambda'\Lambda}^S(\phi''\theta''0)}. \quad (\text{A39})$$

We have restored the spin notation S , since Eqs. (A38) and (A39) are general and hence apply to arbitrary spin S , including $S = 0$.

REFERENCES

- [1] L. D. Faddeev, Sov. Phys. JETP **12**, 1014 (1961).
- [2] W. Glöckle, et. al., Phys. Rep. **274**, 107 (1996).
- [3] A. Arriaga, V. R. Pandharipande, R. B. Wiringa, Phys. Rev. **C52**, 2362 (1995).
- [4] J. Carlson and R. Schiavilla, Rev. of Modern Physics **70**, 743 (1998).
- [5] Ch. Elster, et. al., Few-Body Systems **27**, 83 (1999).
- [6] W. Schadow, Ch. Elster, W. Glöckle, Few-Body Systems **28**, 15 (2000).
- [7] I. Fachruddin, Ch. Elster, and W. Glöckle, Phys. Rev. C **62**, 044002 (2000).
- [8] D. L. Prout, et.al., Phys. Rev. **C65**, 034611 (2002).
- [9] T. Wakasa, et.al., Phys. Rev. **C59**, 3177 (1999).
- [10] H. Kamada, et.al., Phys. Rev. **C66**, 044010 (2002).
- [11] B. D. Keister and W. N. Polyzou, Adv. Nucl. Phys. **20**, 225 (1991).
- [12] W. Glöckle, *The Quantum Mechanical Few-Body Problem* (Springer Verlag, Berlin, 1983)
- [13] M. E. Rose, *Elementary Theory of Angular Momentum* (Wiley, New York, 1957).
- [14] R. Fong and J. Sucher, J. Math. Phys. **5**, 456 (1964).
- [15] W. Glöckle, T.-S. H. Lee, F. Coester, Phys. Rev. **C33** 709 (1986).
- [16] D. Hüber, et. al., Few-Body Systems **22**, 107 (1997).
- [17] R. Machleidt, Adv. Nucl. Phys. **19**, 189 (1989).
- [18] R. B. Wiringa, V. G. J. Stoks, R. Schiavilla, Phys. Rev. **C51**, 38 (1995).
- [19] H. Witała, J. Golak, private communications.
- [20] W. N. Polyzou and W. Glöckle, Few-Body Systems **9**, 97 (1990).
- [21] X. Y. Chen, et.al., Phys. Rev. **C47**, 2159 (1993).

FIGURES

FIG. 1. The spin averaged differential cross section $\frac{d^2\sigma}{dE_nd\theta}$ [mb/(MeV · sr)], the analyzing power A_y and the polarization-transfer coefficient D_{sl} for the (p,n) charge exchange process at projectile energy $E_{lab} = 100$ MeV and neutron laboratory scattering angle $\theta_{lab} = 13^\circ$. The solid line represents the 3D calculation, the dashed line the PW calculation with $j = 7, J = 31/2$. Both calculations are based on the Bonn-B potential [17].

FIG. 2. Same as Fig. 1, but for projectile energy $E_{lab} = 197$ MeV. The solid line represents the 3D calculation, the dashed and dotted lines represent PW calculations with different 2N total angular momentum j and total 3N angular momentum J as indicated in the figure. All calculations are based on the Bonn-B potential.

FIG. 3. The spin averaged differential cross section $\frac{d^2\sigma}{dE_nd\theta}$ [mb/(MeV · sr)], the analyzing power A_y and the polarization-transfer coefficient D_{ll} for the (p,n) charge exchange process at projectile energy $E_{lab} = 197$ MeV and neutron laboratory scattering angle $\theta_{lab} = 24^\circ$. The solid (short dashed) line represent the 3D calculations for the first order term based on the AV18 (Bonn-B) potential. The long-dashed (dotted) lines stand for the partial wave based, full Faddeev calculations based on the AV18 (Bonn-B) potentials. The data are taken from Ref. [17].

FIG. 4. The same as in Fig. 3, but for the spin averaged differential cross section $\frac{d^2\sigma}{dE_nd\theta}$ [mb/(MeV · sr)], the analyzing power A_y and the polarization-transfer coefficient D_{ss} at $\theta_{lab} = 37^\circ$.

FIG. 5. The spin averaged differential cross section $\frac{d^2\sigma}{dE_nd\theta}$ [mb/(MeV · sr)] and the analyzing power A_y for the (p,n) charge exchange process at projectile energy $E_{lab} = 100$ MeV and neutron laboratory scattering angle $\theta_{lab} = 24^\circ$. The solid (short dashed) line give the nonrelativistic 3D calculations for the first order term based on the AV18 (Bonn-B) potential. The long-dashed (dotted) lines represent the 3D calculations that include the effects of relativistic kinematics.

FIG. 6. The spin averaged differential cross section $\frac{d^2\sigma}{dE_nd\theta}$ [mb/(MeV · sr)], the analyzing power A_y and the polarization-transfer coefficient D_{ll} for the (p,n) charge exchange process at projectile energy $E_{lab} = 197$ MeV and neutron laboratory scattering angle $\theta_{lab} = 24^\circ$. The solid (short dashed) line give the nonrelativistic 3D calculations for the first order term based on the AV18 (Bonn-B) potential. The long-dashed (dotted) lines represent the 3D calculations that include the effects of relativistic kinematics. The data are taken from Ref. [17].

FIG. 7. The same as in Fig. 6, but for the spin averaged differential cross section $\frac{d^2\sigma}{dE_nd\theta}$ [mb/(MeV · sr)], the analyzing power A_y and the polarization-transfer coefficient D_{ss} at $\theta_{lab} = 37^\circ$.

FIG. 8. The spin averaged differential cross section $\frac{d^2\sigma}{dE_n d\theta}$ [mb/(MeV · sr)], the analyzing power A_y and the polarization-transfer coefficient D_{sl} for the (p,n) charge exchange process at projectile energy $E_{lab} = 346$ MeV and neutron laboratory scattering angle $\theta_{lab} = 22^\circ$. The solid (short dashed) line give the nonrelativistic 3D calculations for the first order term based on the AV18 (Bonn-B) potential. The long-dashed (dotted) lines represent the 3D calculations that include the effects of relativistic kinematics. The data are taken from Ref. [9].

FIG. 9. The spin averaged differential cross section $\frac{d^2\sigma}{dE_n d\theta}$ [mb/(MeV · sr)], the analyzing power A_y and the polarization-transfer coefficient D_{ll} for the (p,n) charge exchange process at projectile energy $E_{lab} = 495$ MeV and neutron laboratory scattering angle $\theta_{lab} = 18^\circ$. The solid (short dashed) line give the nonrelativistic 3D calculations for the first order term based on the AV18 (Bonn-B) potential. The long-dashed (dotted) lines represent the 3D calculations that include the effects of relativistic kinematics. The data are taken from Ref. [21].

Fig. 1

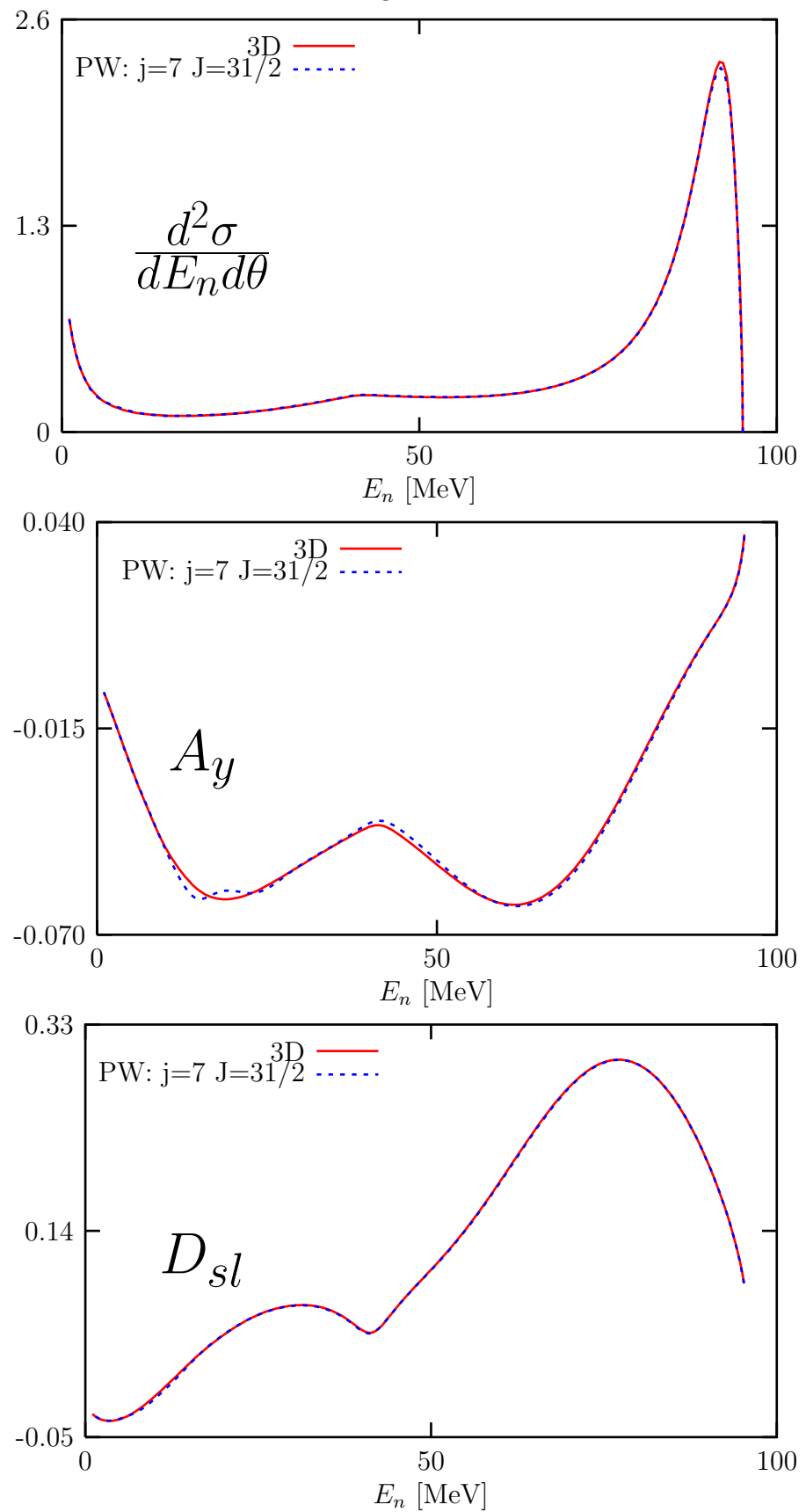


Fig. 2

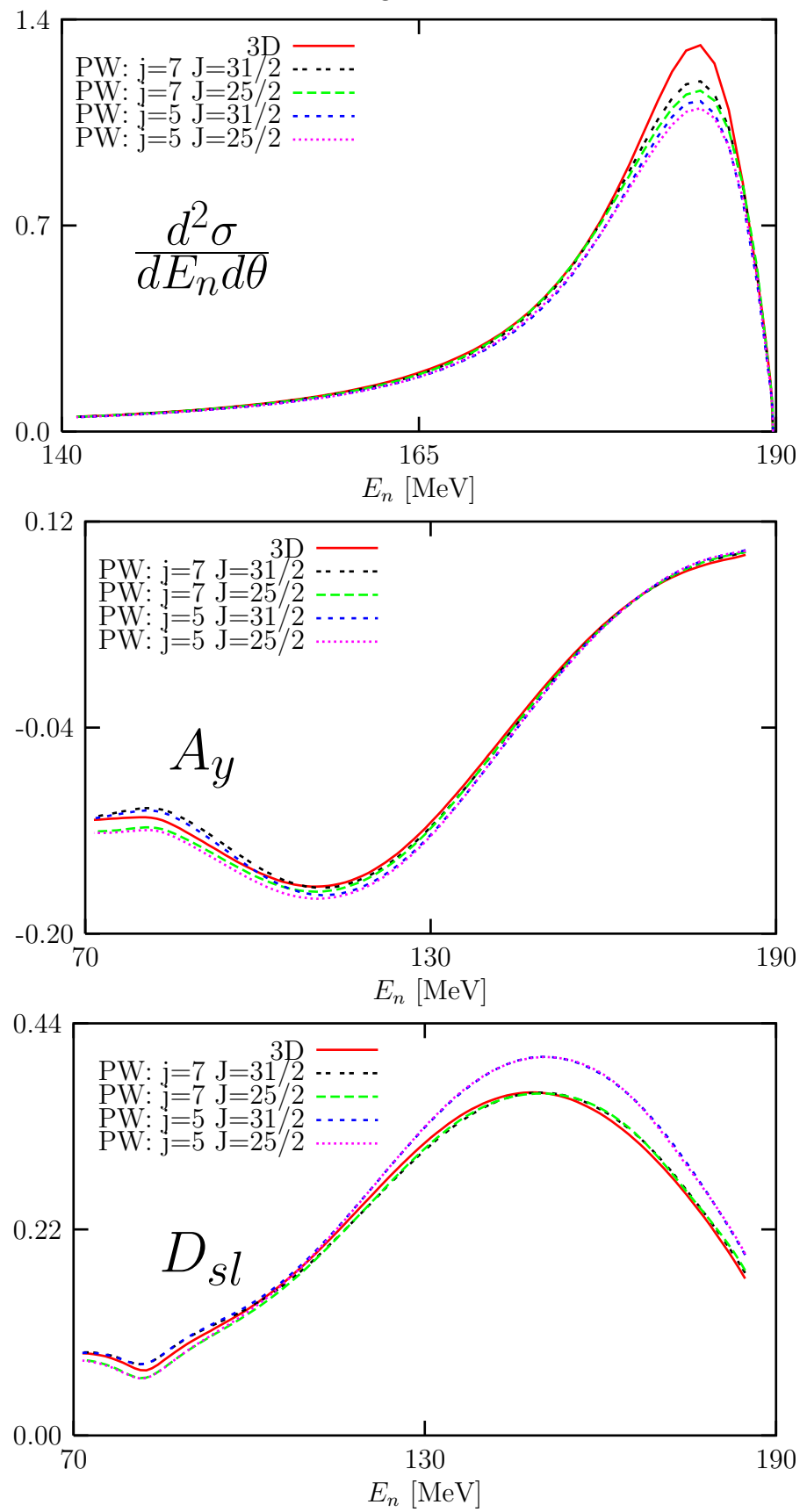


Fig. 3

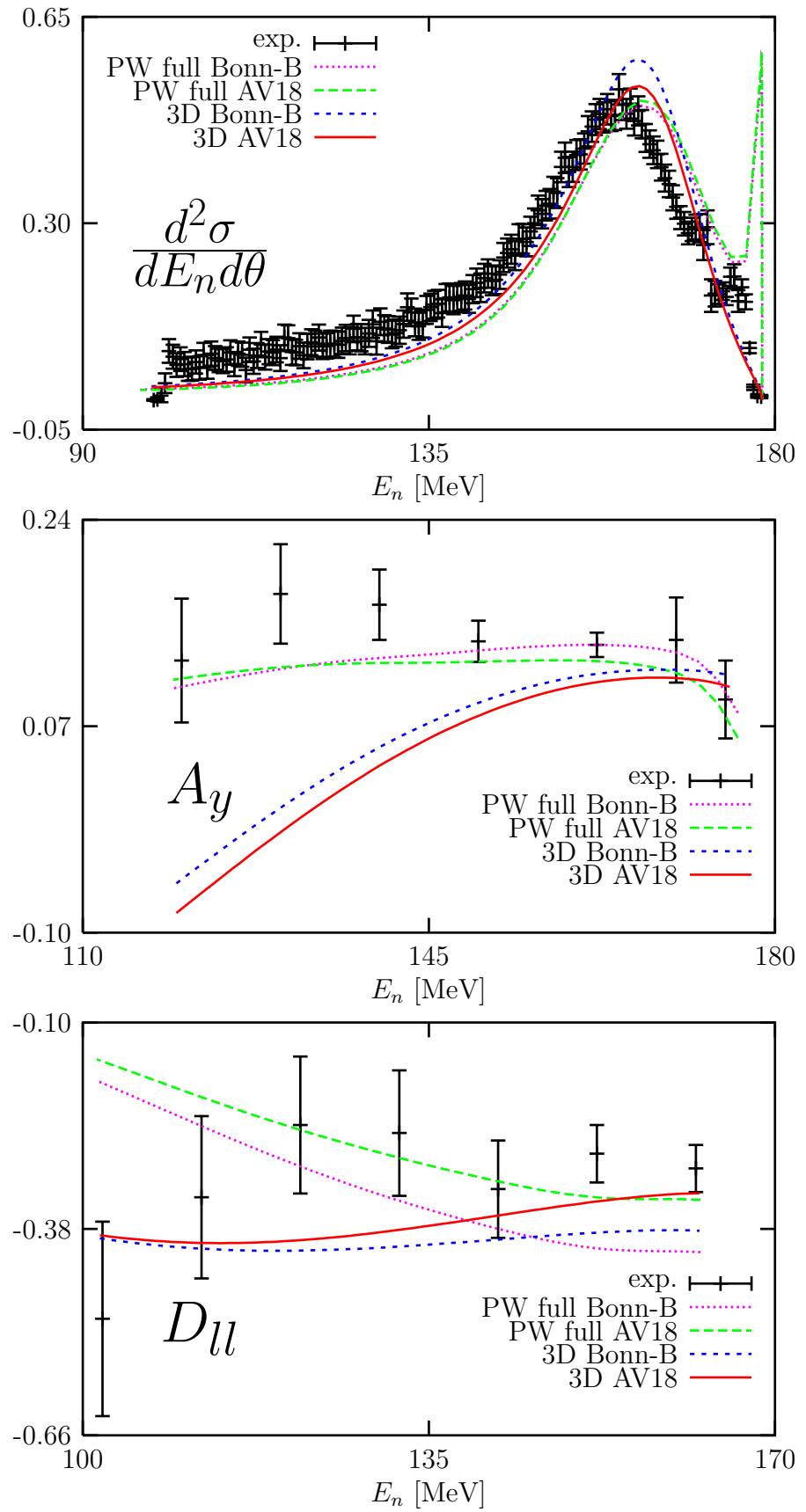


Fig. 4

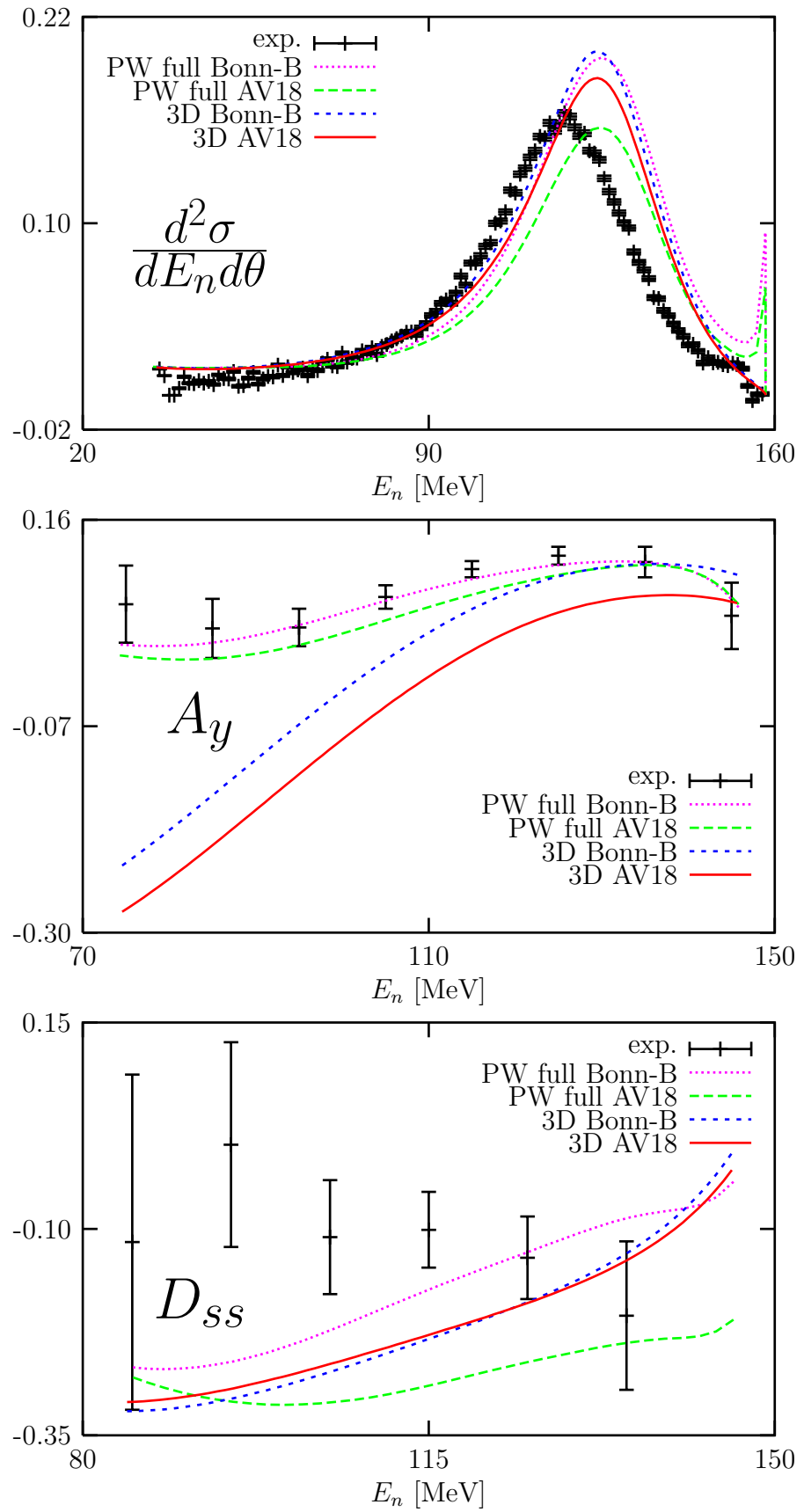


Fig. 5

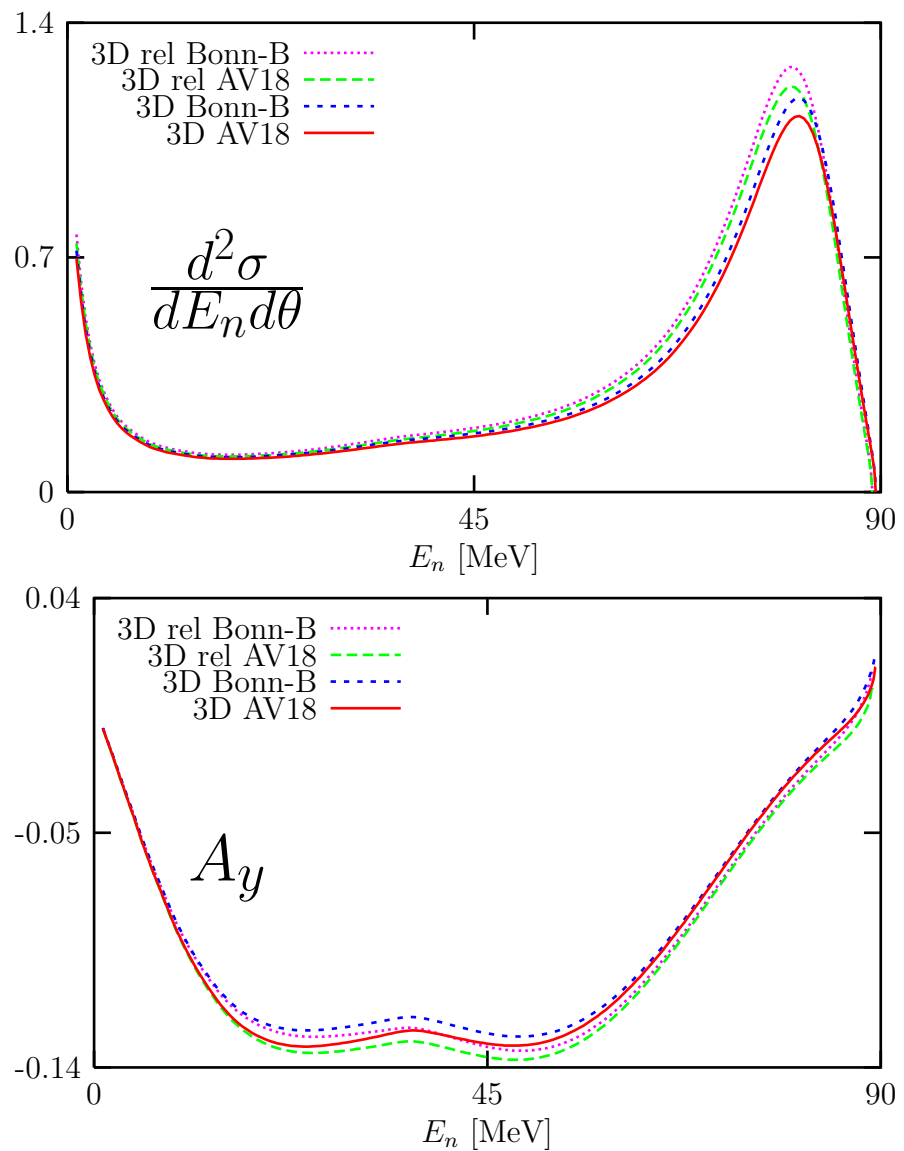


Fig. 6

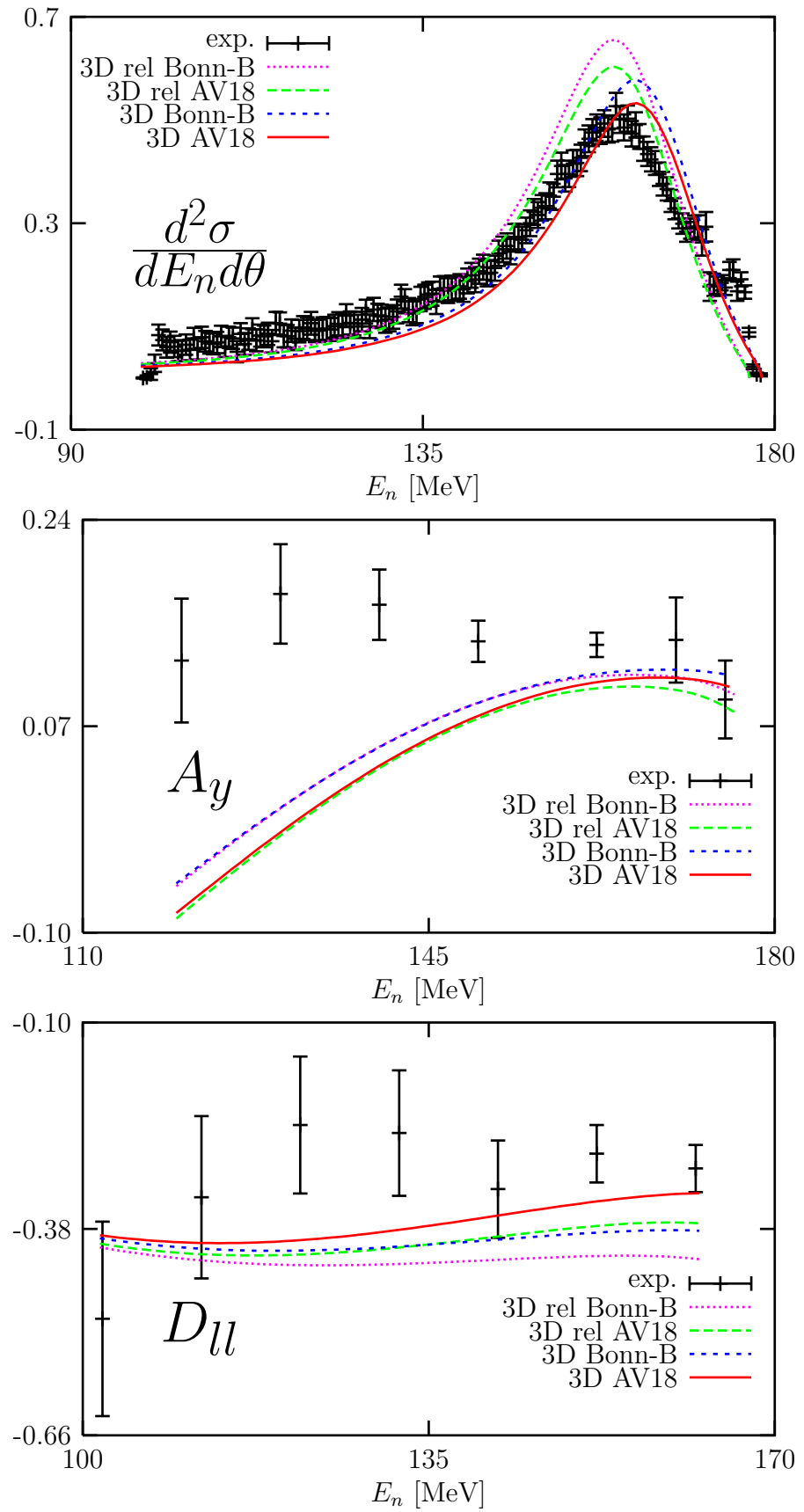


Fig. 7

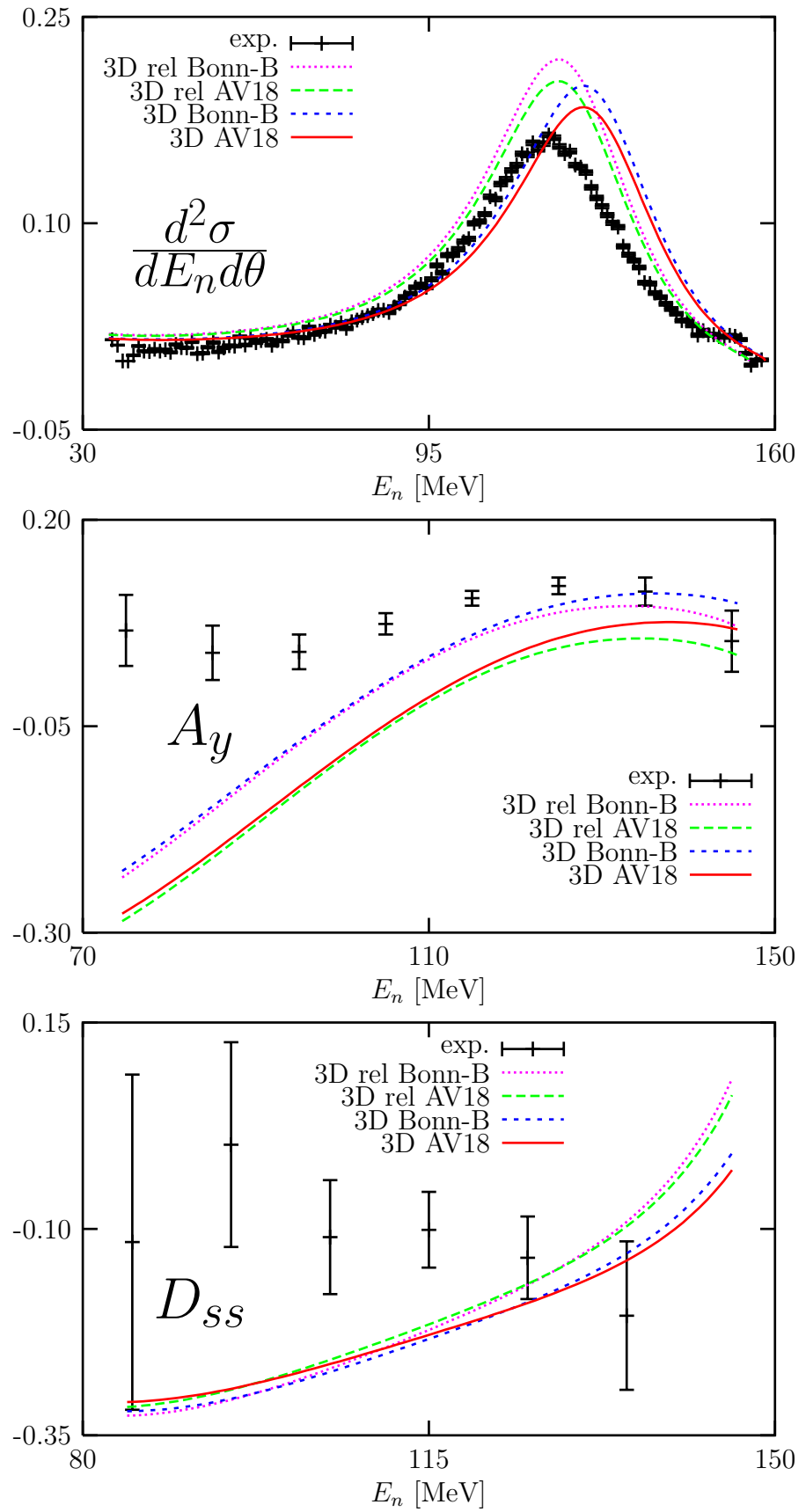


Fig. 8

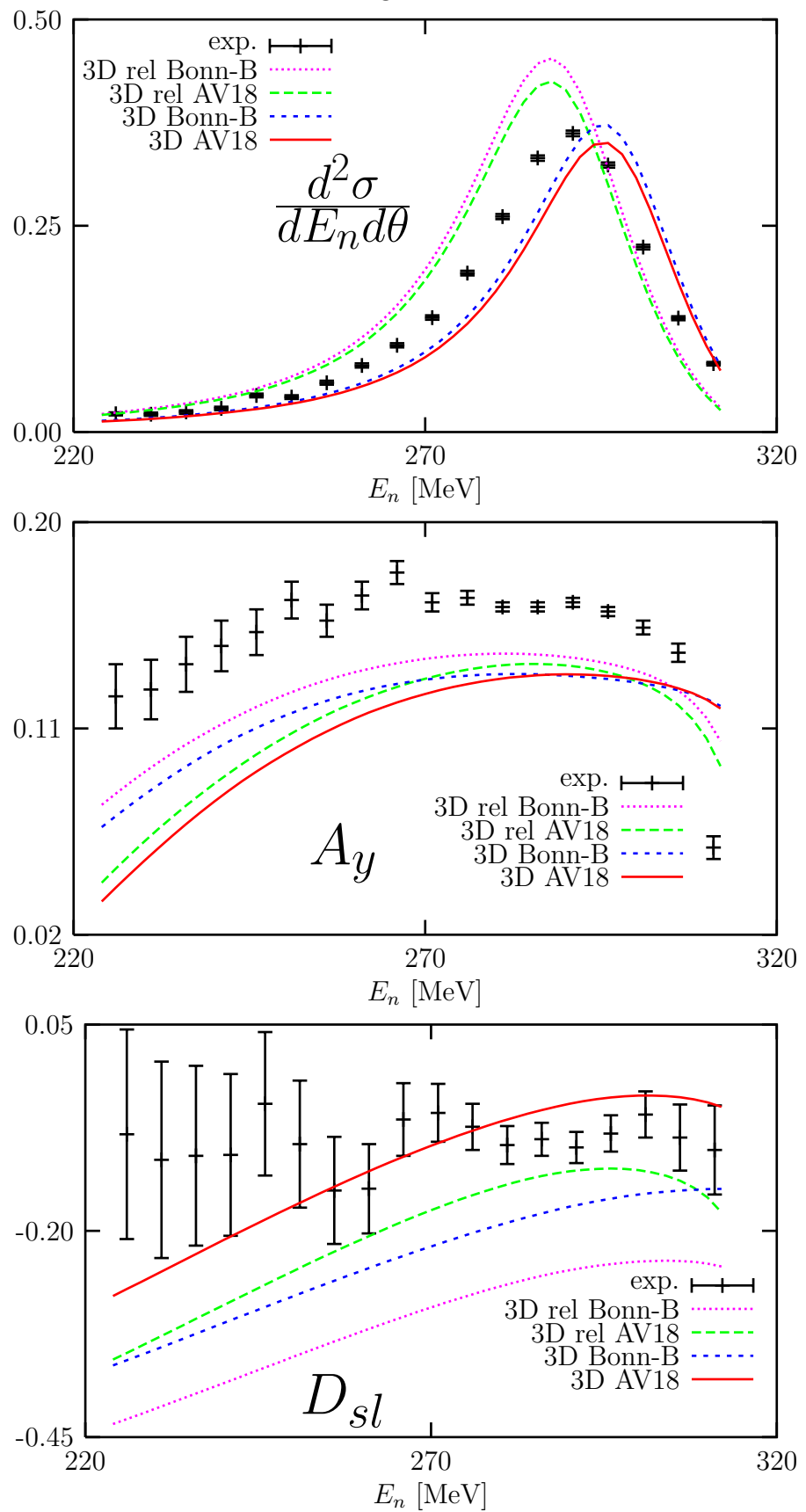


Fig. 9

